AD-A045 656 VIRGINIA POLYTECHNIC INST AND STATE UNIV BLACKSBURG --ETC F/G 20/11
AN INVESTIGATION OF EDGE DAMAGE DEVELOPMENT IN QUASI-ISOTROPIC --ETC(U)
SEP 77 D O STALNAKER, W W STINCHCOMB F33615-75-C-5119
UNCLASSIFIED VPI-E-77-24 NL

1 OF 1
AD A045656

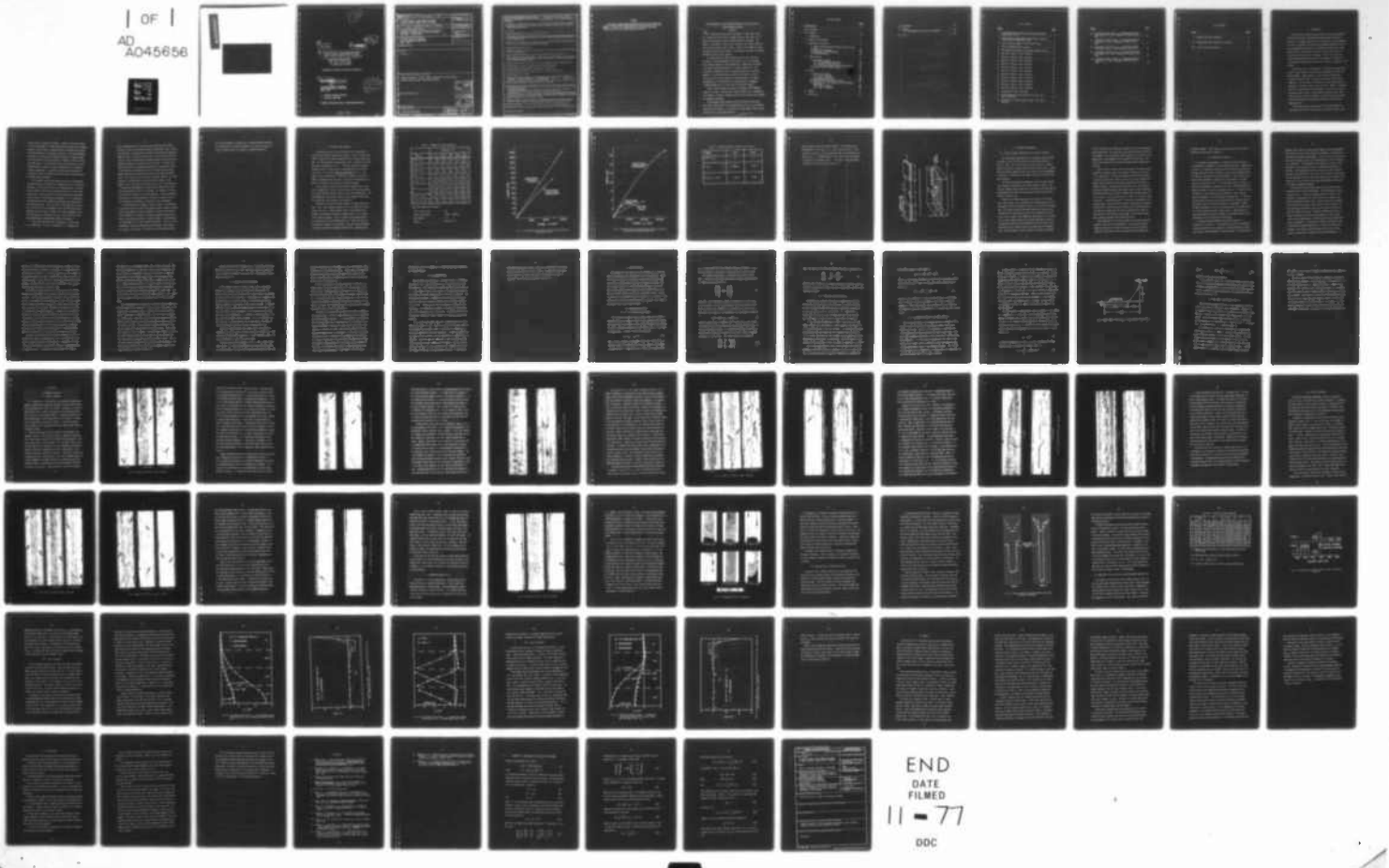

END
DATE FILMED
11-77
DDC

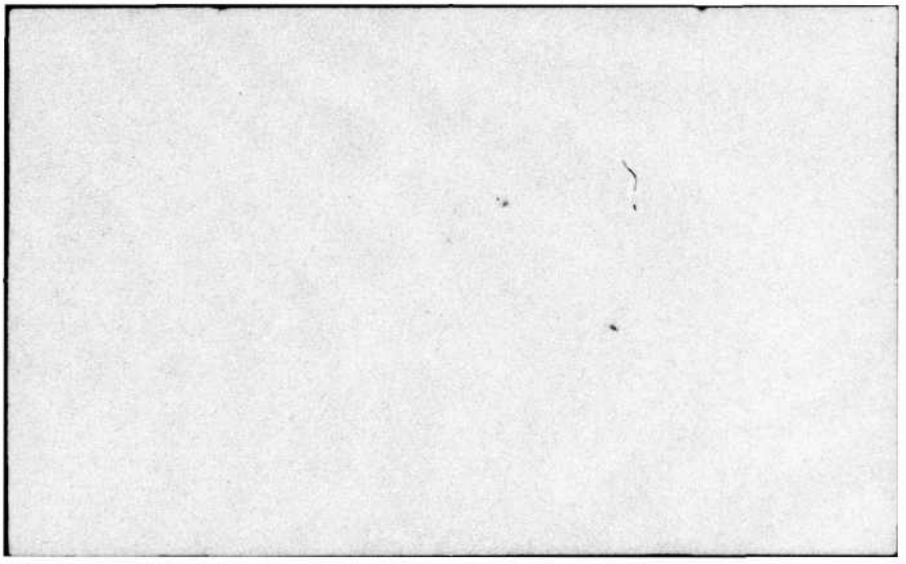

(2)

(12) 91 p.

(14) VPI-E-77-24

(11) Sep[redacted]77

(6) AN INVESTIGATION OF EDGE DAMAGE DEVELOPMENT IN QUASI-ISOTROPIC GRAPHITE EPOXY LAMINATES

(10) David O./Stalnaker
Wayne W./Stinchcomb

Department of Engineering Science and Mechanics

(9) Interim Report
AFML Contract/F33615-75-C-5119
(15)

AIR FORCE MATERIALS LABORATORY
WRIGHT PATTERSON AIR FORCE BASE
OHIO, 45433

1. GRADUATE RESEARCH ASSISTANT
2. ASSOCIATE PROFESSOR

APPROVED FOR PUBLIC RELEASE, DISTRIBUTION UNLIMITED.

404 722

BIBLIOGRAPHIC DATA SHEET	1. Report No. VPI-E-77-24	2.	3. Recipient's Accession No.
4. Title and Subtitle AN INVESTIGATION OF EDGE DAMAGE DEVELOPMENT IN QUASI-ISOTROPIC GRAPHITE EPOXY LAMINATES			5. Report Date September, 1977 6.
7. Author(s) DAVID O. STALNAKER AND WAYNE W. STINCHCOMB			8. Performing Organization Rept. No. VPI-E-77-24
9. Performing Organization Name and Address VIRGINIA POLYTECHNIC INSTITUTE AND STATE UNIVERSITY DEPARTMENT OF ENGINEERING SCIENCE AND MECHANICS BLACKSBURG, VIRGINIA 24061			10. Project/Task/Work Unit No. 11. Contract/Grant No. AFML F33615-75-C-5119
12. Sponsoring Organization Name and Address AIR FORCE MATERIALS LABORATORY WRIGHT PATTERSON AIR FORCE BASE OHIO 45433			13. Type of Report & Period Covered 14.

15. Supplemenrary Notes

16. Abstracts

SEE PAGE ii

17. Key Words and Document Analysis. 17o. Descriprors

Composite materials, fatigue, damage, delamination, quasi-isotropic, laminate, graphite epoxy, load-history effects.

17b. Identifiers/Open-Ended Terms

17c. COSATI Field/Group

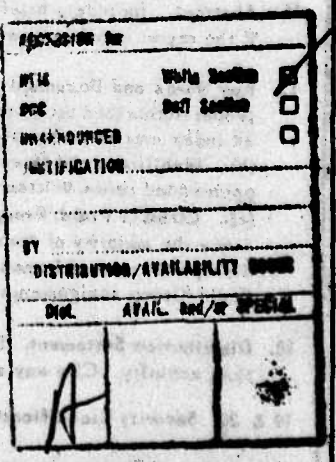

18. Availability Statement	19. Security Class (This Report)	21. No. of Pages
DISTRIBUTION UNLIMITED	UNCLASSIFIED	89
	20. Security Class (This Page) UNCLASSIFIED	22. Price

INSTRUCTIONS FOR COMPLETING FORM NTIS-35 (Bibliographic Data Sheet based on COSATI Guidelines to Format Standards for Scientific and Technical Reports Prepared by or for the Federal Government, PB-180 600).

1. **Report Number.** Each individually bound report shall carry a unique alphanumeric designation selected by the performing organization or provided by the sponsoring organization. Use uppercase letters and Arabic numerals only. Examples FASEB-NS-73-87 and FAA-RD-73-09.

2. Leave blank.

3. **Recipient's Accession Number.** Reserved for use by each report recipient.

4. **Title and Subtitle.** Title should indicate clearly and briefly the subject coverage of the report, subordinate subtitle to the main title. When a report is prepared in more than one volume, repeat the primary title, add volume number and include subtitle for the specific volume.

5. **Report Date.** Each report shall carry a date indicating at least month and year. Indicate the basis on which it was selected (e.g., date of issue, date of approval, date of preparation, date published).

6. **Performing Organization Code.** Leave blank.

7. **Author(s).** Give name(s) in conventional order (e.g., John R. Doe, or J.Robert Doe). List author's affiliation if it differs from the performing organization.

8. **Performing Organization Report Number.** Insert if performing organization wishes to assign this number.

9. **Performing Organization Name and Mailing Address.** Give name, street, city, state, and zip code. List no more than two levels of an organizational hierarchy. Display the name of the organization exactly as it should appear in Government indexes such as Government Reports Index (GRI).

10. **Project/Task/Work Unit Number.** Use the project, task and work unit numbers under which the report was prepared.

11. **Contract/Grant Number.** Insert contract or grant number under which report was prepared.

12. **Sponsoring Agency Name and Mailing Address.** Include zip code. Cite main sponsors.

13. **Type of Report and Period Covered.** State interim, final, etc., and, if applicable, inclusive dates.

14. **Sponsoring Agency Code.** Leave blank.

15. **Supplementary Notes.** Enter information not included elsewhere but useful, such as: Prepared in cooperation with . . . Translation of . . . Presented at conference of . . . To be published in . . . Supersedes . . . Supplements . . . Cite availability of related parts, volumes, phases, etc. with report number.

16. **Abstract.** Include a brief (200 words or less) factual summary of the most significant information contained in the report. If the report contains a significant bibliography or literature survey, mention it here.

17. **Key Words and Document Analysis. (a). Descriptors.** Select from the Thesaurus of Engineering and Scientific Terms the proper authorized terms that identify the major concept of the research and are sufficiently specific and precise to be used as index entries for cataloging.
(b). Identifiers and Open-Ended Terms. Use identifiers for project names, code names, equipment designators, etc. Use open-ended terms written in descriptor form for those subjects for which no descriptor exists.
(c). COSATI Field/Group. Field and Group assignments are to be taken from the 1964 COSATI Subject Category List. Since the majority of documents are multidisciplinary in nature, the primary Field/Group assignment(s) will be the specific discipline, area of human endeavor, or type of physical object. The application(s) will be cross-referenced with secondary Field/Group assignments that will follow the primary posting(s).

18. **Distribution Statement.** Denote public releasability, for example "Release unlimited", or limitation for reasons other than security. Cite any availability to the public, other than NTIS, with address, order number and price, if known.

19 & 20. **Security Classification.** Do not submit classified reports to the National Technical Information Service.

21. **Number of Pages.** Insert the total number of pages, including introductory pages, but excluding distribution list, if any.

22. **NTIS Price.** Leave blank.

FOREWARD

This report documents work performed for the Air Force Materials Laboratory under Contract AFML F33615-75-C-5119, monitored by Dr. N.J. Pagano. The effects of load-history and associated edge damage (transverse cracks and delaminations) are reported.

An Investigation of Edge Damage Development in Quasi-Isotropic Graphite/Epoxy Laminates

Abstract

This investigation describes and documents in detail the initiation, growth, and interactions of damage along the free edges of two types of graphite/epoxy fiber-reinforced composite laminates. The damage is initiated by tensile static loading of flat coupons from each type to three different stress levels. Growth of the damage was caused by tension-tension fatigue loading. The laminates that were investigated differed only by stacking sequence.

The observations were made through the use of the replication technique, a method developed for the purpose of this investigation. This technique allows for three-dimensional, instantaneous recordings of the entire specimen edge while it is under maximum load. The recordings or impressions can be studied microscopically and photographed. This method provides for detail and an overall field of vision that has not been obtained in previous studies. The damage development was also monitored by two non-destructive techniques; vibrothermography and an ultrasonic-pulse echo method.

After a selected number of cycles, the specimens were statically loaded to fracture. Characteristic fracture patterns were observed for each laminate. Residual strength and final elastic modulus were recorded for comparative purposes.

An approximate stress analysis based on laminated plate theory and a more sophisticated finite element analysis were used to determine the stress distributions. A correlation was made between these stresses and the types of edge damage observed.

Table of Contents

List of Figures

List of Tables

1. Introduction

Fiber-reinforced composites have become the most promising material for meeting future requirements for high strength, low weight structures. Presently, much research on composites is being conducted by aircraft, automotive, and even sporting goods manufacturers as well as the Department of Defense and the National Aeronautical and Space Administration. Many aspects of material behavior with respect to various load histories are still unknown. A more exacting science using improved investigative and analytical methods is needed to increase design reliability and to make use of the full advantages of composites.

The purpose of this investigation is to observe and document the growth of edge damage for quasi-isotropic graphite/epoxy (G/Ep) composite coupons. Graphite/epoxy is one of the more common fiber-reinforced composites and is presently being used in many aircraft components. The free edges of the material are most susceptible to damage due to the high stresses that form there. Damage is initiated by tensile static loading of the specimens to various stress levels and then caused to grow by tension-tension fatigue cycling. Observations include the types of damage or cracking that occur and their growth and interactions with respect to the stress levels and repeated cycling.

Much time and effort have been put into the accumulation of large amounts of data on various aspects of material behavior, and,

more recently, on composite materials. However, the primary purpose of this investigation is to make detailed observations of basic damage modes on a small number of specimens and not to accumulate more data. The main objectives are to develop a method of accurately documenting the effect of load history on damage development in composite materials and provide a detailed description of damage initiation, growth, and interactions. The observations that are made should aid in the understanding of changes in material response such as strength and stiffness degradation. In addition, observations concerning the occurence and growth of damage are necessary before accurate analytical models can be developed.

The uniqueness of the observations made for this investigation centered around the development of a method known as the replication technique. This technique allows for three-dimensional, instantaneous recordings of the entire specimen edge while it is still under maximum load. These recordings can then be studied microscopically and any areas of interest can be photographed. This technique permits observations with two important advantages over those made in many previous studies. Since the replicas are made while the specimen is under full load, much damage can be seen that would not be apparent after the load is released. The second advantage is that the entire edge is recorded and not just a small portion as when the specimen edge is photographed through a microscope.

It has been observed by many investigators, in particular, G. C. Grimes (Ref. 1) and K. L. Reifsnider, E. G. Henneke, and

W. W. Stinchcomb (Ref. 2), that the stress-strain behavior of G/Ep laminates contain significant and distinct proportional limits. Grimes has found that "in studies done for the Air Force Materials Laboratory (AFML: TR-75-33, TR-73-311, and TR-72-40) the tension static test proportional limit of graphite/epoxy laminates denotes the onset of micromechanical damage in the form of matrix cracking." To further investigate and describe the phenomena that causes the proportional limit, the stress levels that were chosen for this particular study represented stresses below, approximately equal to, and above the proportional limit stresses for the particular laminates studied. For these laminates, the proportional limits are actually "knees" in what appears to be a bi-linear axial stress-strain curve. The differences in the observed edge damage will then be used to determine any significant developments that occur at the knee. The change in stiffness at the knee was characteristic of each laminate. These two laminates differed only by stacking sequence, therefore, the question of how this influences the sharpness of the knee will be investigated.

Direct observation of damage at interior regions of the material is much more difficult to make than along the edges. However, studies are being performed at Virginia Polytechnic Institute and State University (VPI&SU) in an attempt to relate the damage observed on the edge of the specimen with that in interior regions. Two non-destructive techniques will be used in this investigation. The first, vibrothermography, indicates "delamination type" damage in the plane of the specimen. The second, an ultrasonic pulse-echo method, detects

real-time development of damage under a specimen-mounted transducer. The investigation and results discussed in this report are part of a study of defect-property relationships in composite materials.

2. Materials and Specimens

The specimens used in this investigation were constructed of Hercules Type A/S 3501 graphite-epoxy prepreg. Table 1 indicates the material properties at various temperatures for a unidirectional laminate. All room temperature (approximately 70°F) properties are from the material manufacturer (Ref. 3). Stiffness properties have been adjusted slightly to agree with the room temperature stress-strain curves (Fig. 1-2) from the Composite Design Guide (Ref. 4). The changes in each property due to temperature changes are from Ref. 5; however, adjustments have been made so that the room temperature properties will agree with the previously quoted references.

It was necessary to obtain these material properties as a function of temperature in order to perform stress analyses which account for residual thermal stresses caused by high curing temperatures. The room temperature stress-strain curves are also needed as input data for a non-linear finite element stress analysis.

Specimens of two quasi-isotropic geometric configurations were used. Type I had a stacking sequence of $[0, \pm 45, 90]_s$ while Type II was $[0, 90, \pm 45]_s$. These two types clearly illustrated the differences in the amounts and types of damage that occur as a result of the stacking sequence. Table II contains some average mechanical properties of the two laminates (Ref. 2). These two types are of particular interest to study because, even with large differences in laminate properties and damage characteristics, laminated plate

Table I. Summary of AS-3501 Properties

	Temperature (°F)					
Property	-67°	70°	180°	260°	300°	350°
E_1^T (10^6 · psi)	21.0	20.8	20.4	20.2	20.1	20.0
E_2^T (10^6 · psi)	1.45	1.43	1.35	1.22	1.14	0.88
E_1^C (10^6 · psi)	17.1	16.9	16.5	16.3	16.2	16.1
E_2^C (10^6 · psi)	1.52	1.50	1.42	1.29	1.21	0.95
G_{12} (10^6 · psi)	0.88	0.86	0.81	0.75	0.68	0.31
ν_{12}	0.28	0.28	0.28	0.28	0.28	0.28
ν_{21}	0.022	0.022	0.021	0.019	0.018	0.015
α_1(10^{-6} ·in/in/°F)	-0.30	-0.20	-0.13	-0.05	-0.02	+0.01
α_2(10^{-6} ·in/in/°F)	10.3	13.0	15.0	16.6	17.8	19.6

Other Room Temperature Properties

Fiber volume percent. 62%

Cured ply thickness . . . . . 0.0052 $\pm$ .0004 in.

Void content. . . . . < 2%

Density . . . . . 0.057 lb/in.^{3}

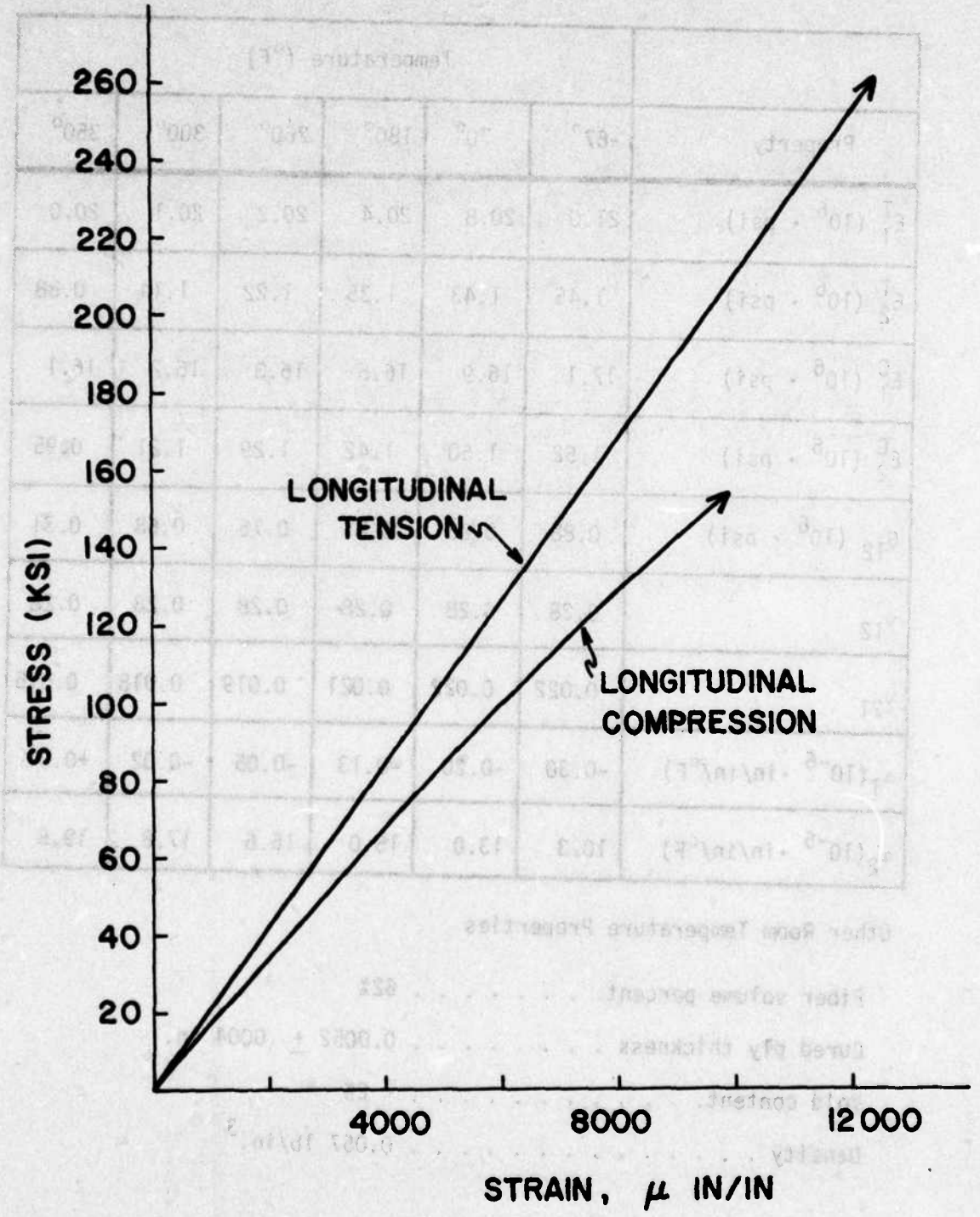

Fig. 1 Longitudinal Stress-Strain Curves for Unidirectional AS-3501 G/Ep at 70°F.

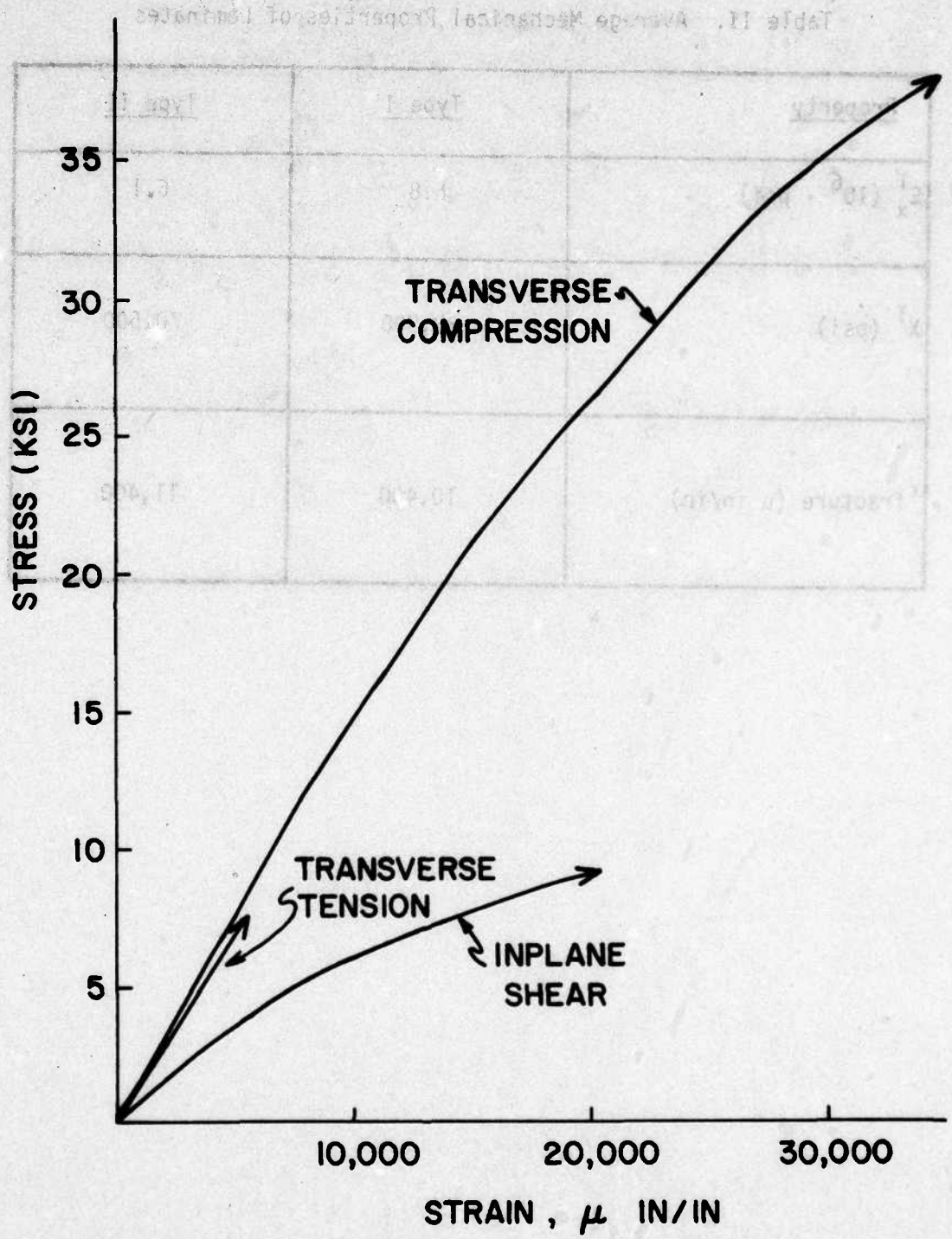

Fig. 2 Transverse and In-plane Shear Stress-Strain Curves for Unidirectional AS-3501 G/Ep at 70°F.

Table II. Average Mechanical Properties of Laminates

Property	Type I	Type II
E_x^T (10^6 · psi)	6.8	6.1
X^T (psi)	68,800	70,500
$\epsilon_{fracture}$ (μ in/in)	10,400	11,400

theory predicts identical in-plane stresses. All specimens were approximately 7.0 in. long, 1.0 in. wide, and 42 mils thick. Each specimen also had 2.0 in. glass epoxy end tabs with tapered ends, as shown in Fig. 3. The orientations of the fibers within each lamina are defined in terms of an angle θ. This angle is measured counter-clockwise from the axial direction (Fig. 4).

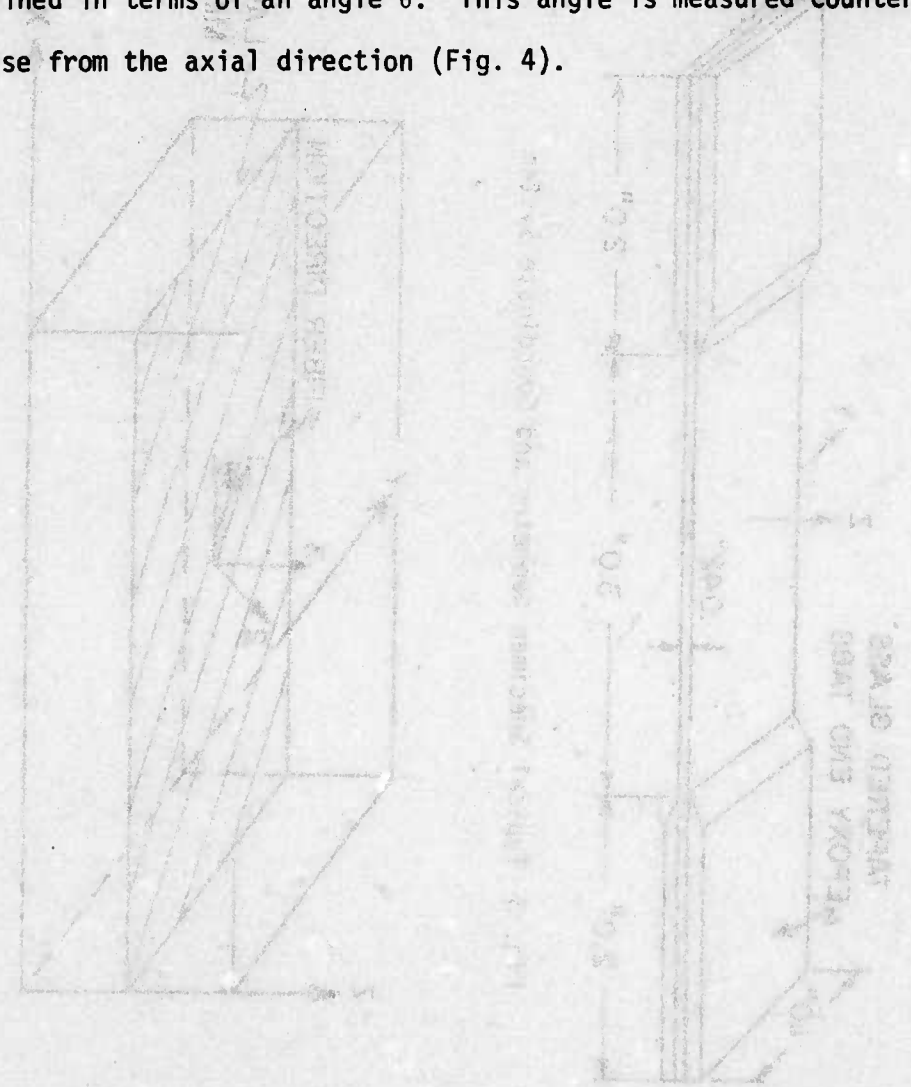

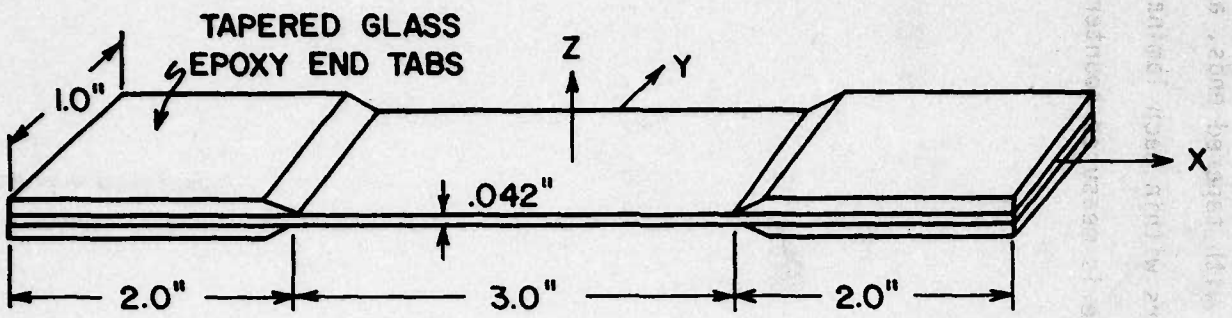

Fig. 3 Typical Specimen Geometry and Coordinate System

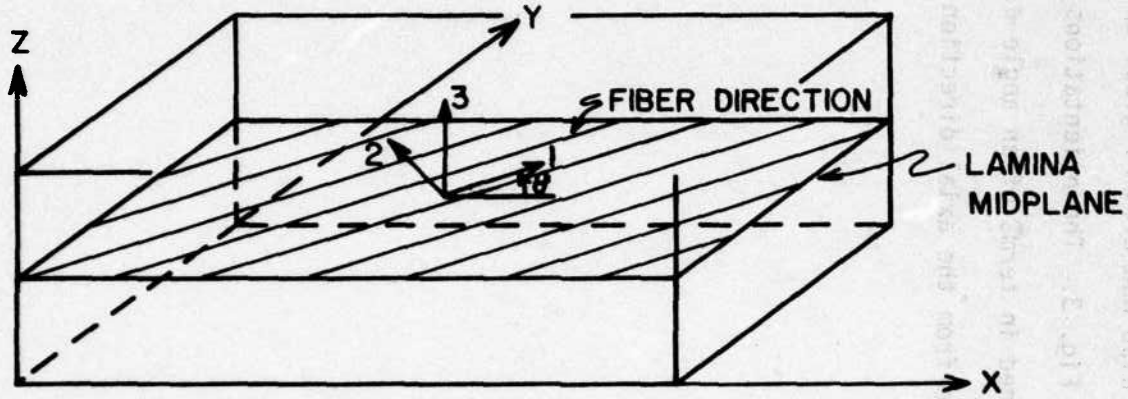

Fig. 4 Fiber Orientation Within a Lamina

3. Experimental Procedures

3.1 Static Preload, Fatigue Cycling, and Final Fracture

This investigation required only six specimens; three of which were Type I, $[0, \pm 45, 90]_s$, and the other three were Type II, $[0, 90, \pm 45]_s$. One from each type was quasi-statically loaded to 1600 lb or 38.5 ksi, slightly below the stress-strain knee. A second pair was loaded to 2000 lb or 48.0 ksi, which is in the neighborhood of the knee. The third pair was loaded to 2700 lb or 64.9 ksi, well above the knee.

The static preloads were conducted on a 20 kip Instron machine at a crosshead displacement rate of 0.05 inches per minute. Each test was stopped after reaching 200 lb and again at the full load for approximately ten minutes for the purpose of making replicas (discussed in Section 3.2).

Strain was recorded continuously from three, one inch long, axial strain gages. Two of the gages were mounted adjacent to the free edges and the third gage was located in the center of the specimen. The original idea of using three gages was to record any differential strain that might occur due to the propagation of transverse cracks. However, the attempt was unsuccessful in this respect. It was later recognized that any resulting differential strains on the specimen surface would be undetectable due to the small crack openings and their location within the middle layers of the specimen. The three gages did reveal important information concerning

initial stiffnesses and differential strains resulting from unsymmetric loading conditions. The conditions could possibly have been caused by misalignment of the cross-heads, uneven gripping of the specimen by the wedge grips, or misalignment of the specimen within the grips. Most probably the differential strains were caused by some combination of the three.

After the static preloads, the strain gages were removed and each specimen was fatigued using an extensometer to measure strain over a 1.0 in. gage length. Testing was performed on a MTS servo-hydraulic, closed-loop machine with a tensile capacity of 20 kips. Material responses were continuously monitored by a Tektronix WP 1100 data acquisition system. By sampling load and strain data, the system calculated and recorded maximum load, maximum strain, dynamic compliance, dissipated energy, and the specific damping ratio at preselected numbers of cycles. All cycling was done at a rate of 1.0 Hz and a stress ratio of 0.1. The maximum stress, in each case, corresponded to the preload stress. All the 1600 lb and 2000 lb specimens were fatigued 10,000 cycles, and 500 cycles were applied to the 2700 lb specimens. The tests were stopped after 50, 500, and 5000 cycles in order to make replicas of the loaded specimen edges. For the 2700 lb specimens, replicas were made after 50 and 100 cycles.

Upon completion of the fatigue loading, strain gages were again mounted in the center of each specimen. The specimens were then loaded to failure at the same rate used for the static preloads. Load-strain curves were plotted to determine final stiffness and

residual strengths. These results, as well as the results from the replicas, are discussed in Chapter 5.

3.2 Replication Technique

In the study of edge damage it is essential to have a quick, reliable method of permanently recording damage occurrences. Without such a method it is impossible to make extensive microscopic examination of the edges and draw reliable conclusions concerning load-damage history. An essential requirement of any such technique is that it must be capable to being performed on specimens that are mounted in a testing machine and subjected to load. This requirement makes it possible to monitor the development of damage due to static or fatigue loadings by making recordings at intervals throughout the test. In addition, these recordings or replicas made while the specimen is under load will contain the damage in its most enlarged or opened state. If the replication was made after the load was removed from the specimen, many of the smaller cracks would close and perhaps go undetected. Another necessary requirement is that the technique possess sufficient resolution to allow detection of the smallest cracks. Magnifications of forty power appear sufficient to detect all transverse cracks and delaminations as well as individual fiber bundles.

A suitable recording method was devised and used by K. L. Reifsnider, et al (Ref. 2). This technique consists of a camera and microscope fastened to the crosshead of a testing machine by a mount which permits vertical movement of the microscope. At given intervals

during a static test, the loading may be stopped and the displacement held constant while the entire edge of the specimen is scanned and all interesting developments photographed. Also, a particular location may be observed throughout the test and photographed to record the damage as it progresses. The advantage of this technique is that it allows continuous visual observation as well as permanent photographic recordings. The disadvantages are that only one very small section of one edge can be observed at a given time, that scanning an entire edge is time consuming, and that areas which prove to be of interest in the latter part of the test may not have been photographed in their earlier stages of damage development.

The replicating technique developed for this research effort eliminates many of these disadvantages. The development was done by the author and J. E. Masters, a graduate student at VPI&SU. This technique is adapted from one used in transmission electron microscopy for duplicating small areas of surfaces that are not suitable for use with the microscope. These replicas, which are made from cellulose acetate replicating tape, have sufficient resolution for even the electron microscope. After much experimenting with different thicknesses of tape and various methods of taking impressions from the specimen edge, a relatively simple and reliable technique was developed. The impression is made by softening one side of the tape with acetone and pressing it against the edge of the specimen. The surface of the tape remains soft for only a few seconds; therefore, the impression must be made immediately. In

addition, the impression must be made without any slippage of the replicating tape along the edge of the specimen. If slippage does occur, the image will be blurred. It was found that the best way to make instantaneous impressions without slippage was to fasten a strip of the replicating tape in place along the specimen edge before applying any acetone. This was done by simply attaching the ends of the replicating tape to the specimen with adhesive tape.

The problem of evenly applying the acetone along the interface between the specimen edge and replicating tape required much effort to solve. The best method found was injecting an even stream of acetone along the interface with a hypodermic syringe. The small needle did not disturb the mounted tape and the syringe permitted excellent control of the flow of acetone. Immediately following the injection of acetone, a small amount of pressure is applied with the finger to the back of the tape to make the impression. Replicating tape with a thickness of ten mils made the best impressions since it was thick enough to allow for a deep impression and still retain its basic shape without excessive buckling or tearing when peeled off and handled. After the tape is removed from the specimen, it is mounted between glass slides which keep it flat and free of fingerprints and dirt.

Replicas can be made as often as desired throughout a static or fatigue test simply by stopping the test for a few minutes to allow time for making the replica. After the test is completed, the replicas contain a complete history of the damage as it developed along the specimen edges. The replicas are then scanned and studied

microscopically, and photographs made of any places of interest. One principle advantage of the replicas is that they are transparent and can be placed in a photographic enlarger in the place of a negative. The prints for this research project (Fig. 6-16) were made in this manner. The enlarger used was a 35 mm Durst, condensing type, enlarger. Selected sections as well as the entire replica can be printed. The prints of the entire replica are pieced together and mounted to give an excellent overall picture of the damage along that edge. The prints made in this report are magnified approximately 40 times. When the entire edge is printed, the resulting picture is about ten feet long.

One disadvantage of the technique is that the replicas themselves are not always free of defects. If care is taken in the making of the impressions, the defects present, if any, will be of little significance. Three types of defects occurred. The first type was bubbles or circular voids. These were caused by excessive amounts of acetone that were not squeezed out as pressure was applied along the back of the replicating tape. The second type of defect consisted of irregularly shaped areas that were void of any impressions. These areas were caused by a lack of acetone. The third type of defect was caused by uneven pressure applied along the back of the replicating tape. This caused deeper impressions in some areas than in others. The result was contrasting areas of light and dark on the photographs. All three of these defects can be seen in Fig. 6, however, they will be pointed out and discussed in Section 5.1.

Replicas were made of both edges of all six specimens while they were held at the full static load. Additional replicas were made at various intervals throughout the fatigue tests. The results are discussed in Section 5.1.

3.3 Ultrasonic Pulse-Echo Method

In an attempt to monitor internal damage growth, a technique known as the ultrasonic pulse-echo method was employed (Ref. 2). Pulsed ultrasonic waves were continuously passed through the specimens during the static and fatigue tests. The development of damage in the material below the transducer serves as a diffraction grating and therefore reduces the amplitudes of the returning echoes. An apparent attenuation is calculated and recorded based on the amplitudes of the first two echoes. This attenuation is not a function of the energy adsorption of the specimen but is a function of the dispersion of the wave due to diffraction caused by damage. Also, it is dependent on the adsorption of the delay block and on bond losses, but these affects should remain relatively constant throughout the test.

Reference 2 reported data that showed rises in the apparent attenuation for static tests to failure of about 0.7 db/echo for these same types of graphite/epoxy materials. It also indicates sharp rises in the neighborhood of the stress-strain knee.

The specimen was placed between a 0.5 in., 5 MH_z ceramic transducer and a 1.0 in. fused quartz delay block using stop-cock grease as a bonding agent. The delay block separated the echoes so that they

would be individually distinguishable as well as serving as a transmission line for the diffracted waves. A Matec 9000 Pulse Generator generated the ultrasonic waves and a Matec Attenuation Recorder, Model 2470A, electronically compared the peaks of the first two returning echoes from each pulse.

In this investigation, the results were not as conclusive as those reported for static loading (Ref. 2). Only the 1600 lb and 2700 lb, Type I specimens showed significant rises in attenuation. The 1600 lb specimen had a 0.25 db/echo rise between 1400 and 1600 lb. In the case of the 2700 lb specimen there was a total rise of 0.56 db/echo, however, there were no sharp rises as expected in the area of the knee. The fatigue data was not consistent and no atempts were made to draw any conclusions from it.

The lack of consistent data may have been caused by changes in the bond thickness. It has not been determined if the thickness of the bondline remains constant. If it were changing, its effects on the attenuation would be so large that the small decreases due to damage development in the material would not be noticeable. For some of the specimens at lower loads there may not have been any damage development under the transducer. At the time of the test, the location of the transducer on the specimen was not recorded. This makes it impossible to draw any specific comparisons between the amount of damage present on the replicas and the attenuation recorded. In conclusion, this portion of the investigation was unsuccessful; perhaps because of the method itself, but most

probably due to lack of experience in using the pulse-echo technique for fatigue studies.

3.4 Vibrothermography

The specimens were examined by a technique known as vibrothermography after their static preloads and again after fatigue cycling. This technique, first introduced at VPI&SU, was recently developed by T. S. Jones (Ref. 6) and has been proven as an effective non-destructive method of detecting delaminations in this kind of material. The specimens were mounted in a magneto-strictive transducer which was driven by a 200 watt ultrasonic generator with a frequency range of 17.4-21.0 kHz. Energy was put into the specimens by means of axial vibrations. Any delaminations present in the specimens dissipated a portion of this energy in the form of heat. An AGA 680 Thermovision thermographic camera was used to observe the resulting surface heat patterns.

It was noted that certain areas will dissipate heat at one frequency but others will not. Therefore, the entire frequency range of the generator was scanned in order to determine the frequencies at which each specimen was the most responsive. In addition, removing a specimen from the transducer and then remounting it changed these frequencies. This fact made the comparison of the "hot spots" present before and after fatigue somewhat more difficult. The size of any given hot spot was not only a function of the frequency but also of the length of time that the specimen was vibrated. In conclusion,

the comparisons had to be made on the basis of the number of hot spots present and the location of their centers. No comparisons were made with respect to the size of any area or the frequency at which it occurred. The results are discussed in Section 5.2.

4. Stress Analyses

The stresses that are present in the specimens due to the three axial load conditions were determined by two stress analyses. These stresses were obtained in an attempt to understand and explain the occurences of damage observed with the replication technique. The first analysis served as a "first approximation" and is based on plane-stress laminated plate theory with approximate method of calculating residual thermal stresses and interlaminar normal stresses. A second, more sophisticated analysis was used for the purpose of comparison and for obtaining interlaminar shear stresses. This analysis was based on the finite element method.

4.1 Approximate Analysis

4.1.1 Thin Laminated Plate Theory

The simplest and quickest stress analysis that can be made on a composite material is based on classical thin laminated plate theory. The simplicity of this theory largely results from making the assumption that a laminate, subjected to axial loading only, is in a state of plane stress. A state of plane stress requires

$$\sigma_z = \tau_{xz} = \tau_{yz} = 0, \qquad (1)$$

where the axis system is illustrated in Fig. 3-4. Plane stress is commonly assumed for materials of this type. However, even though σ_z might be small in comparison to σ_x, it may still cause failures

such as delaminations when the strength through-the-thickness is low. This is discussed in more detail in the third part of this section.

The following development of laminated plate theory is from Ref. 7. Considering each individual lamina to behave orthotropically, the stress-strain relationship is

$$\begin{Bmatrix} \sigma_x \\ \sigma_y \\ \tau_{xy} \end{Bmatrix} = [\bar{Q}] \begin{Bmatrix} \varepsilon_x \\ \varepsilon_y \\ \gamma_{xy} \end{Bmatrix}, \tag{2}$$

where $[\bar{Q}]$ is the transformed reduced stiffness matrix of the lamina. If the assumptions of small displacements, small displacement gradients, and plane strain are made, the stress-strain relationship for each layer with respect to the deformations of the assembled laminate is

$$[\sigma]^k = [\bar{Q}]^k [\varepsilon_o] + z [\bar{Q}]^k [\kappa], \tag{3}$$

where the superscript "k" denotes the k^{th} layer and $[\varepsilon_o]$ and $[\kappa]$ are the midplane strains and curvatures of the laminate, respectively. In most practical applications, it is desirable to define a relationship between these strains and curvatures and the total stress and moment resultants of the laminate. This relationship can be defined as

$$\begin{Bmatrix} N \\ M \end{Bmatrix} = \begin{bmatrix} A & B \\ B & D \end{bmatrix} \begin{Bmatrix} \varepsilon_o \\ \kappa \end{Bmatrix}, \tag{4}$$

where [N] and [M], the stress and moment resultants, respectively, are

$$\begin{Bmatrix} N \\ M \end{Bmatrix} = \int_{-H}^{H} [\sigma] \begin{Bmatrix} 1 \\ z \end{Bmatrix} dz, \qquad (5)$$

and [A], [B], and [D] are the laminate extensional stiffness, coupling stiffness, and bending stiffness matrices, respectively, and 2H is the laminate thickness.

4.1.2 Residual Thermal Stresses

Graphite-epoxy laminates are cured at a temperature of 350°F. During the cool down stage of the curing process, residual thermal (curing) stresses develop which can make a significant contribution to the total stress field of the material. H. T. Hahn and N. J. Pagano (Ref. 8) point out that for some cases the curing stresses are large enough to cause failure of layers within the laminate.

At the fabrication temperature of 350°F, just as the cool down stage is begun, the layer bonding is nearly complete and the material is solidified, but has a very low stiffness. In accordance with these observations, Hahn and Pagano make the assumption that the material is in a stress free state and that residual stresses begin developing immediately as the material is cooled down. Since the operating temperature of the specimens is 70°F, the change in temperature is -280°F.

For a first approximation of the curing stresses, the following assumptions were made: symmetric laminate, all layers of equal thickness, and constant material properties (independent of temperature).

This yields stresses in each layer of

$$[\sigma]^k = \Delta T\, [\bar{Q}]^T \{[\bar{\alpha}] - [\alpha]^k\}, \qquad (6)$$

where ΔT is the change in temperature, $[\alpha]^k$ is the transformed thermal coefficient of the k^{th} layer, and $[\bar{\alpha}]$, the laminate thermal coefficient, is

$$[\bar{\alpha}] = h\, [A]^{-1} \sum_{k=1}^{n} [\bar{Q}]^k\, [\alpha]^k, \qquad (7)$$

where h is the thickness of a layer and the summation is being made over all layers. The full development of Eq. 6 and 7 is shown in Appendix A. The curing stresses for each layer can now be added to the mechanical stresses as determined by Eq. 2 to give the total stress field.

4.1.3 Interlaminar Normal Stress Approximation

One of the limitations of the stress analysis discussed in this section is that it requires the interlaminar normal and shearing stresses to be zero. The use of this assumption is justified in a "first approximation" type of analysis and yields usable data. However, this assumption breaks down in the vicinities of the free edges of the material. It is fairly well accepted that this area is confined to thin regions which are adjacent to the free edges and have a width approximately equal to the specimen thickness. This concept has been studied and confirmed by N. J. Pagano and R. B. Pipes (Ref. 9) and again by Pipes (Ref. 10), as well as others.

In these regions it is possible for the interlaminar stresses to become sufficiently large to promote failure of the material. Of the interlaminar stresses, σ_z is particularly instrumental in causing delaminations of the layers along the edges of a laminate (Ref. 2). A tensile σ_z stress along an interface near the free edge will tend to cause a pulling apart of the layers at that interface. For this reason it is important to know the sign of the stress (tension or compression) as well as its approximate magnitude. There are many analyses available, most of which use various finite difference or finite element techniques, which will determine the σ_z stresses. One such method is presented in Section 4.2. However, these analyses require much time and expense.

For many purposes a sophisticated, detailed analysis is not needed. N. J. Pagano and R. B. Pipes (Ref. 11) have presented an approximate method to determine the σ_z distribution in the boundary layer regions. The basis of this method is the assumed stress distribution along an interface as shown in Fig. 5. In order to assure through-the-thickness equilibrium along each interface, the ratio of the stresses is determined to be

$$\sigma'_m = \sigma_m/5. \tag{8}$$

To require the moment due to the σ_z stresses to balance the moment created by the σ_y stresses, the maximum stress is

$$\sigma_m = \sigma_m(z) = 45M(z)/14\ H^2 \tag{9}$$

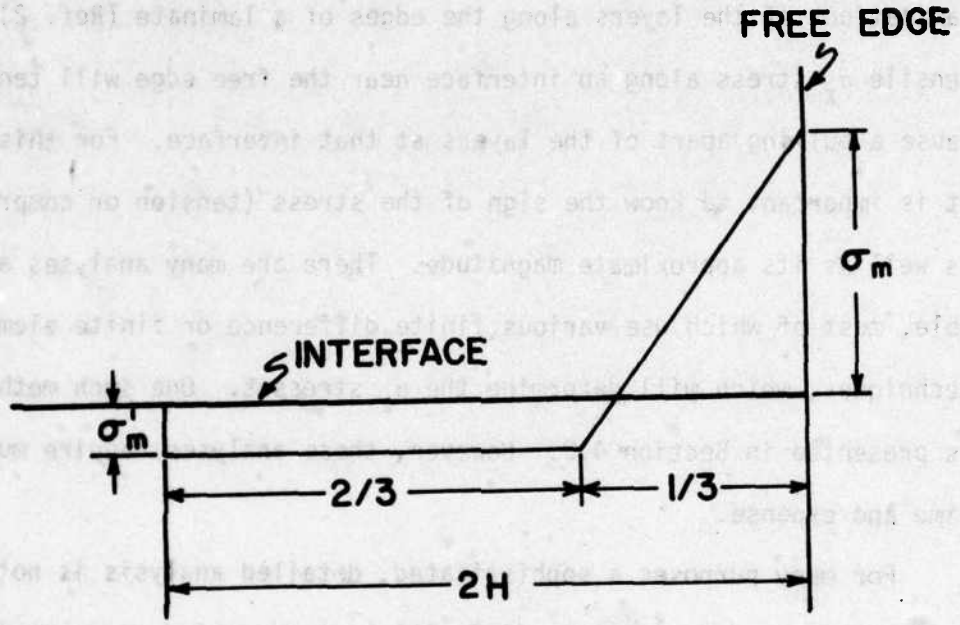

Fig. 5 Approximate Distribution of Interlaminar Normal Stress

and $$M(z) = \int_{z}^{H} \sigma_y(\zeta)\, \zeta\, d\zeta, \qquad (10)$$

where 2H is the laminate thickness.

The σ_y stresses used in Eq. 10 are found from the analysis previously discussed which combined both mechanical and curing stresses. A computer coded program was written to perform the entire operation as well as determine laminate properties. The discussion of the results are in Section 5.4.

4.2 Nonlinear Finite Element Analysis

The previously discussed analysis is very inexpensive and quick to run, computer-wise, and data is easy to determine. However, for the purpose of comparison and also to determine the interlaminar shear stresses, a much more sophisticated finite element analysis was performed. The finite element model, Nonlinear Analysis of Laminated Fibrous Composites, was developed by G. D. Renieri and C. T. Herakovich (Ref. 12) and modified by E. H. Humphreys (Ref. 13).

This technique was specifically developed for the three-dimensional stress analysis of symmetric, balanced, fiber reinforced composite laminates subjected to axial and thermal loadings. All nonlinear stress-strain behavior of the material is input by using Ramberg-Osgood approximations. Material properties that are a function of temperature are input as percent retention curves. Loading, whether mechanical or thermal, is an incremental process for which

the elements of each layer are capable of having different properties for each increment.

The actual area of the specimen that is modeled or discretized using the finite elements is a cross-sectional plane perpendicular to the axial loading direction. Since the specimen is symmetric and balanced, only a quarter of this cross-section needs to be analyzed. The finite elements used are constant-stress, constant-strain triangular elements. The element grid consisted of 188 elements with the elements near the free edge small enough to allow for a data point (centroid of element) to be within .008 in. of the edge. This permitted a reasonable estimate of the stress distributions along the free edge to be obtained. The results are discussed in Section 5.4.

5. Results

5.1 Results of Replicas

5.1.1 Type I Specimens

G. C. Grimes (Ref. 1) states that he observed no micromechanical damage in graphite/epoxy laminates subjected to static tensile stress below the proportional limit. For the Type I specimens, a significant proportional limit, or knee, is observed in the longitudinal stress-strain curve at a load of about 2000 lb. Therefore, the 1600 lb specimen should contain no cracking after the static preload. However, this is definitely not the case. Figures 6, 7, and 8 illustrate typical damage as well as patterns of fatigue damage growth that were observed at 1600 lb.

Figure 6a represents a 0.20 in. length along the edge of the specimen. Arrow 1 points out one of the four transverse cracks present in this region after the static preload had been applied. These cracks span the two inner 90° layers. The long white lines (arrow 2) are not cracks but are scratches left in the specimen by the cutting process in which the specimens are cut from larger panels. These saw marks are seen in many of the replicas. Figure 6b is of the same location as (a) but after 50 cycles. There are no changes except for a small "hooked" crack (arrow 3) that has branched into one of the inner 45° layers. Arrow 4 points out a piece of dust or lint that has stuck to the replica. Some experience is required to properly

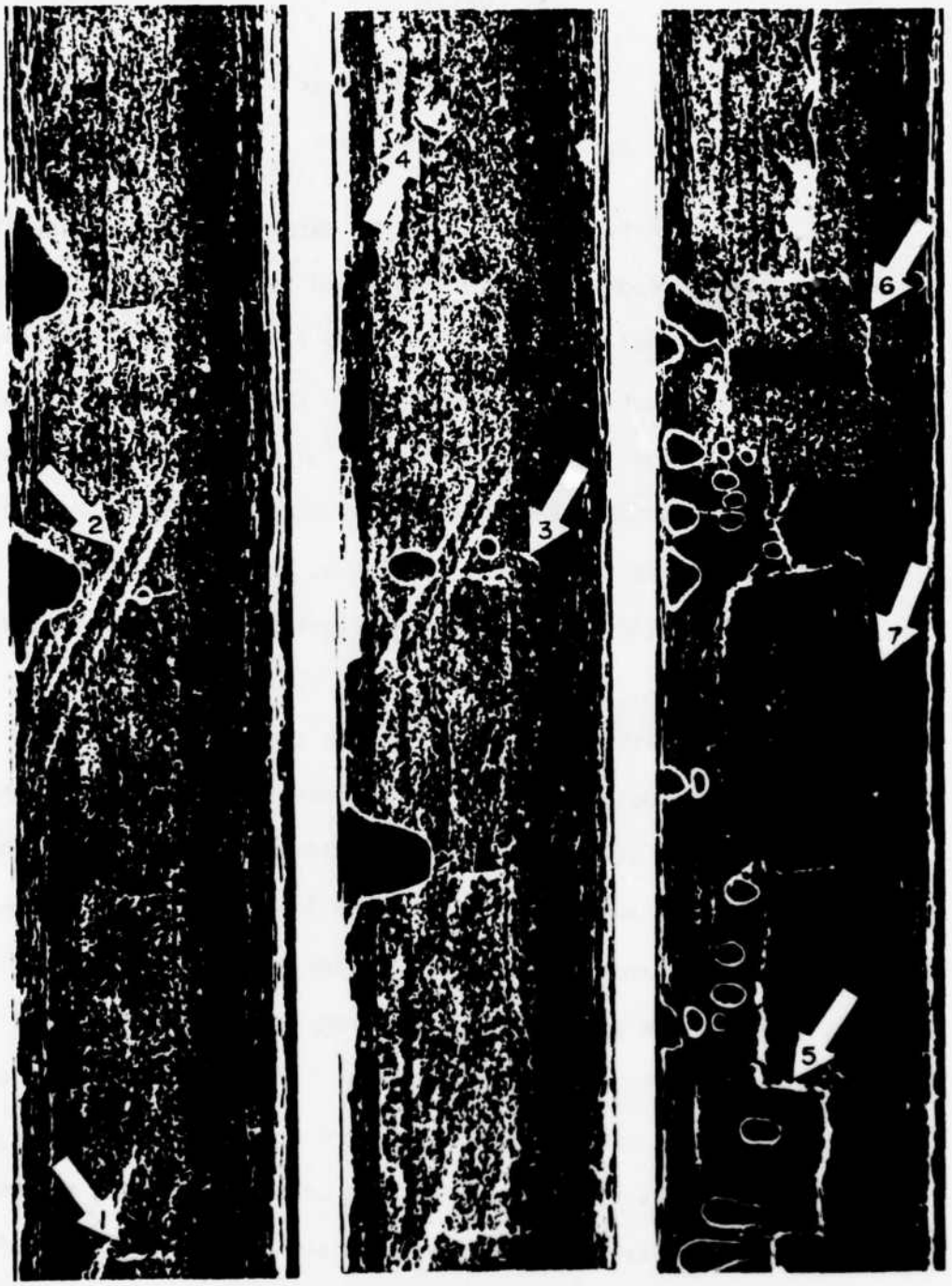

a) Static b) 50 Cycles c) 10,000 Cycles

Fig. 6 Replicas of 1600 lb, Type I Specimen

interpret the information that a replica contains. Confusing areas will be pointed out so that they will not distract from the value of the replication technique itself. As can be seen in Fig. 6c, arrow 5, an additional transverse crack has formed after 10,000 cycles. There is also a delamination along the $-45^{\circ}/90^{\circ}$ interface at the bottom of the picture. A transverse crack has caused it to jump to the opposite $90^{\circ}/-45^{\circ}$ interface and then the crack at arrow 5 has caused it to jump back again. From the top of the picture a delamination along the $90^{\circ}/90^{\circ}$ interface appears to have grown downward until it was stopped by another transverse crack. In this case, instead of jumping to another interface, small "branch" delaminations begin to grow from the tips of the transverse crack along the $+45^{\circ}/-45^{\circ}$ interfaces (arrow 6). The transverse crack below this also has branch delaminations originating from its crack tips as well as a small longitudinal crack which has grown into its center. This longitudinal crack may be the beginning of a major delamination. Other points of interest in this picture are the cracks through the outer $+45^{\circ}$ layers that stem from the branch delaminations. One of these four cracks is pointed out by arrow 7.

Figure 7 contains an excellent illustration of the turning effect that a transverse crack can have on a delamination. Arrow 1, in Fig. 7a, points out a transverse crack with a hooked crack that hooks in the same direction in which the delamination is growing. As a result of this and the fact that the delamination is in the lower $90^{\circ}/-45^{\circ}$ interface, it is turned and forced down into the $-45^{\circ}/+45^{\circ}$

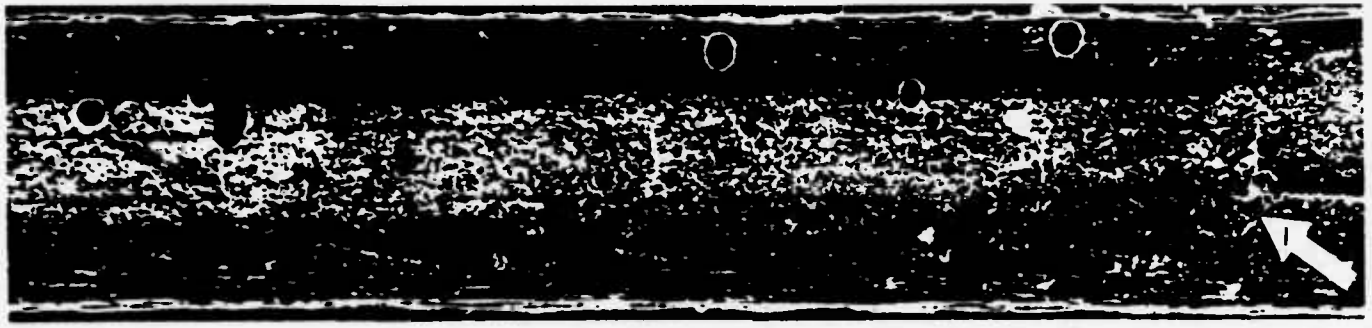

a) 50 Cycles

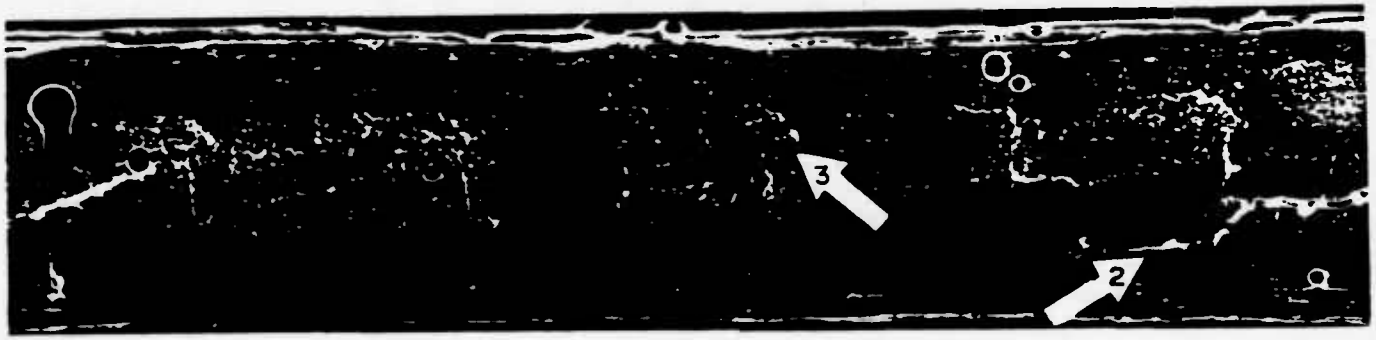

b) 10 000 Cycles

Fig. 7 Replicas of 1600 lb, Type I Specimen

interface (arrow 2). If the delamination had approached the transverse crack from the $90^{\circ}/90^{\circ}$ interface, it probably would have stopped at the crack and caused extensive growth of the branch delaminations. If the hooked crack had turned in the opposite direction from the delamination growth, then the delamination would probably have jumped to the upper $-45^{\circ}/90^{\circ}$ interface. Both of these "if" conditions were illustrated in the previous figure. Also of interest in Fig. 7b are the four transverse cracks that have hooked cracks through the inner -45° layers but which are offset from the crack tip at the $-45^{\circ}/90^{\circ}$ interface (arrow 3 points out one of these).

A third section of this same 1600 lb specimen is shown in Fig. 8. The main purpose of this figure is to illustrate the magnitude of the delamination width at the most severe location. In (a), the delamination growing along the $90^{\circ}/90^{\circ}$ interface from the right hand side has been stopped by a transverse crack and a branch delamination has formed. However, after 10,000 cycles (Fig. 8b), it can be seen that the delamination broke through the crack and continued its growth. As observed earlier, there is no jumping between interfaces due to the transverse crack if the delamination is along the midplane. The branch delamination appears to stop growing when the delamination breaks through the parent transverse crack. Arrows 1 and 2 point out longitudinal cracking that has occurred prior to delamination as seen in (b), these cracks determine the path that the delamination will take. The delaminations from the left and right have continued to grow and finally met at the transverse crack pointed out by arrow 3.

a) 50 Cycles

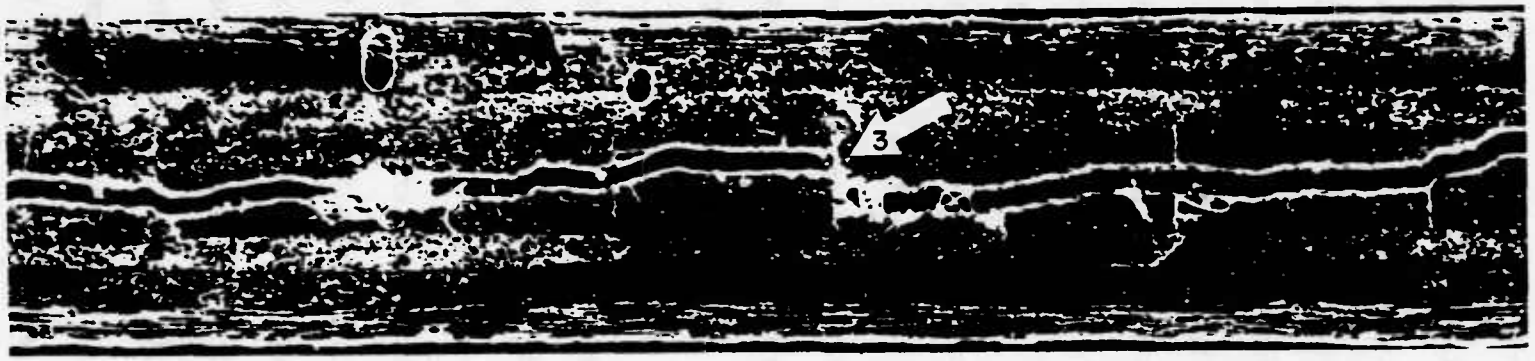

b) 10 000 Cycles

Fig. 8 Replicas of 1600 lb, Type I Specimen

The characteristics of the damage development observed in the 1600 lb specimen are also observed in the 2000 lb specimen, however, some of the individual phenomena and details, such as branch delamination and longitudinal cracking, appear more pronounced. For example, Fig. 9 represents a sequence of events from the 2000 lb specimen. In (a), it can be seen that this particular location on the specimen contained only one transverse crack. After 50 cycles, (b) indicates four, possibly five, transverse cracks, as well as three distinct hooked cracks in the inner -45° layer. One of these (arrow 1) does not appear to be associated with a parent transverse crack. Arrow 2 points out a turning point in the delamination. This may have been caused by a slanted or angle crack, a portion of which is visible above the turning point. After 10,000 cycles, a delamination has grown down from the top and stopped at a transverse crack (arrow 3). A small branch delamination formed; however, the major delamination did not continue. If it had done so, it would have continued straight along the 90°/90° interface. It appears that another delamination, independent of both the upper and lower ones, has bridged the gap between the transverse cracks at arrows 3 and 4. This delamination then caused the long branch delamination. Finally, the lower delamination grew upward to the transverse crack at arrow 4. Arrows 5 and 6 indicate the areas where the specimen fractured. This will be discussed in Section 5.3.

The most extreme case of branch delamination found in the 2000 lb specimen is shown in Fig. 10. Since the delamination did not break through the transverse crack, the branch delaminations had the

a) Static b) 50 Cycles c) 10 000 Cycles

Fig. 9 Replicas of 2000 lb, Type I Specimen

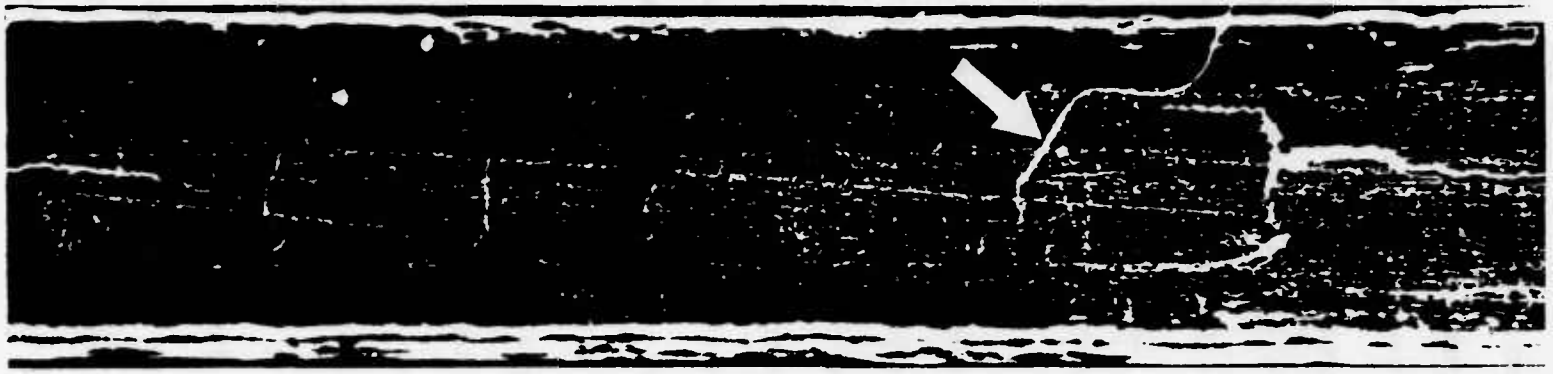

a) 500 Cycles

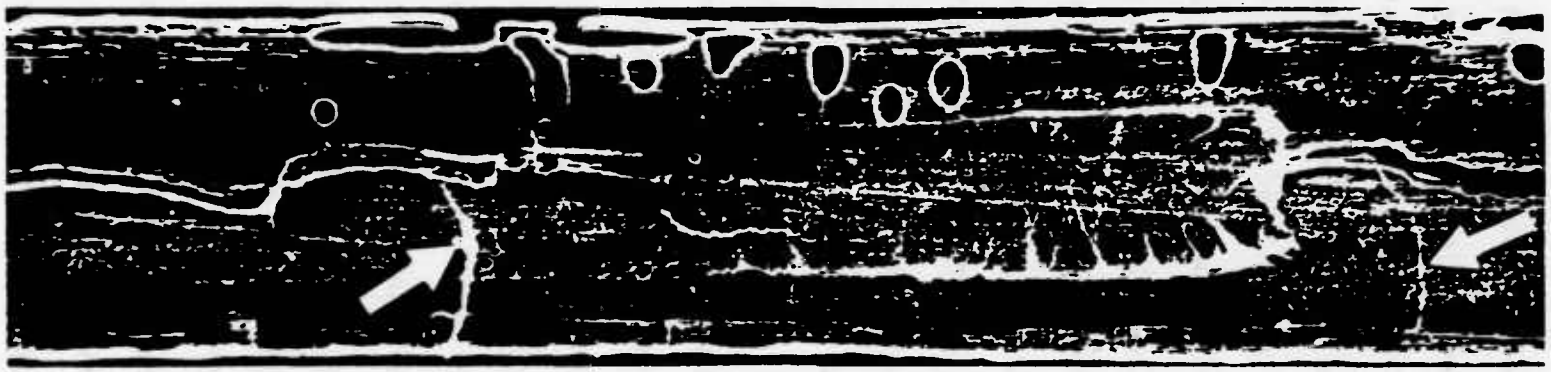

b) 10 000 Cycles

Fig. 10 Replicas of 2000 lb, Type I Specimen

time necessary to grow to such proportions. Consequently, when the specimen was loaded to failure, it fractured at this spot. The three arrows in this figure point out dust or lint that is stuck to the replica and should not be mistaken for cracks.

Figures 11 and 12 are of the 2700 lb specimen. The characteristics of damage development discussed for the previous specimens are found to be the same for this specimen. Even though it was only fatigued for 500 cycles, the amount of damage is similar to the 2000 lb specimen after 10,000 cycles, except that delaminations are more extensive. There is approximately 97 percent delamination for the 2000 lb specimen and 100 percent for the 2700 lb specimen but its maximum crack width is more than twice as large. As can be seen in Fig. 11a, a large number of transverse cracks occur when the specimen is loaded to the static preload. The spacing between these cracks is representative of the entire specimen. It tends to vary from about the thickness of the laminate down to a third of the thickness. No new transverse cracks formed after the preload. It has been observed for all Type I specimens, regardless of load, that once an area has been delaminated, no new transverse cracks are formed. Arrow 1 indicates a slanted or angle crack which influences the path of the delamination, as can be seen in (b). Fig. 12 illustrates the magnitude of the most severe crack opening. The 50 cycle replica is shown here because it is of much better quality than the 500 cycle replica. For this particular specimen, the crack width of the delamination was largest near the center and near the tab regions of the specimen.

a) Static

b) 50 Cycles

Fig. 11 Replicas of 2700 lb, Type I Specimen

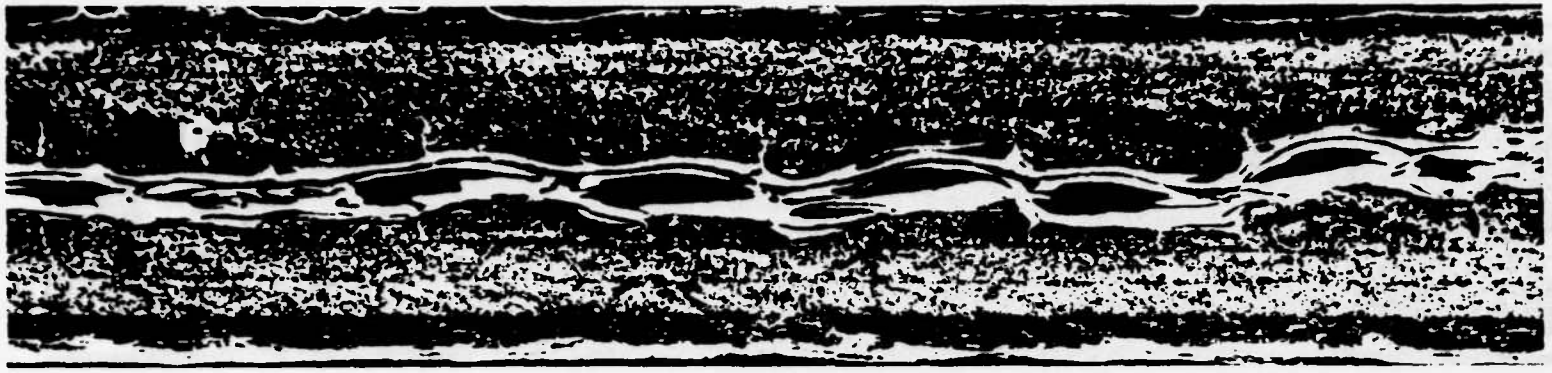

a) Static

b) 50 Cycles

Fig. 12 Replicas of 2700 lb, Type I Specimen

In some experimental work done by G. P. Sendeckyj (Ref. 14), many similar observations were made concerning edge damage development for Type I graphite/epoxy coupons. He observed the jumping of the delaminations between $90^{\circ}/-45^{\circ}$ interfaces, the linking-up of delaminations to form a completely delaminated edge, the increase of delamination crack widths with respect to load, and the occurrence of transverse cracking before delamination. However, his observations did not include the development of delamination along the $90^{\circ}/90^{\circ}$ interface, hooked cracks through the inner -45° layers, or branch delaminations along the $+45^{\circ}/-45^{\circ}$ interface. Also, he does not state that delamination can begin along some portions of the edge while transverse cracking is still taking place elsewhere along the length. At 1600 lb or 59 percent of the ultimate load, the replicas indicated that 22 percent of the specimen edge is delaminated. Sendeckyj did not observe any delamination until 66 percent of the ultimate load was reached for his particular specimens.

Considering that only three Type I specimens were used in this investigation, the replication technique has provided much consistent and valuable information for establishing a chronological development of edge damage. The damage observed was much more complete than microscopic observations of the unloaded specimens or even microscopic scanning of the edges while the specimen is being loaded.

5.1.2 Type II Specimens

In many ways the damage development in Type II specimens is similar to Type I, but there are also many differences. For example, the crack opening or width in Type II material is much smaller and this makes the cracks more difficult to observe. A method, such as the replication technique, which allows observation of the specimen while subjected to maximum load, is essential.

A sequence of photographs of replicas from the 1600 lb, Type II specimen is shown in Fig. 13. The two 90° layers are no longer together, but are adjacent to the two outer 0° layers. As with the Type I material, the first damage that occurs is transverse cracking in the 90° layers. However, the cracks are only half the length of those in the Type I specimens; thus, they are more difficult to observe. Arrows 1 and 2 in (a) point out two of the six, or possibly more, transverse cracks present. An interesting observation is the epoxy-rich area pointed out by arrow 3. This may have been the "joint" between two pieces of prepreg tape that filled with epoxy as the material was cured. After 50 cycles, a few additional cracks have formed, two of which are pointed out by arrows 4 and 5. Similarly, after 10,000 cycles, still more cracks have formed, two of which are indicated by arrows 6 and 7. The spacing of the two cracks at arrow 7 is about the thickness of one layer. This is about three times closer than any transverse cracks observed in the Type I specimens.

A static preload of 2000 lb does not appear to cause much more damage than in the 1600 lb case (Fig. 14a). Arrows 1 and 2 indicate

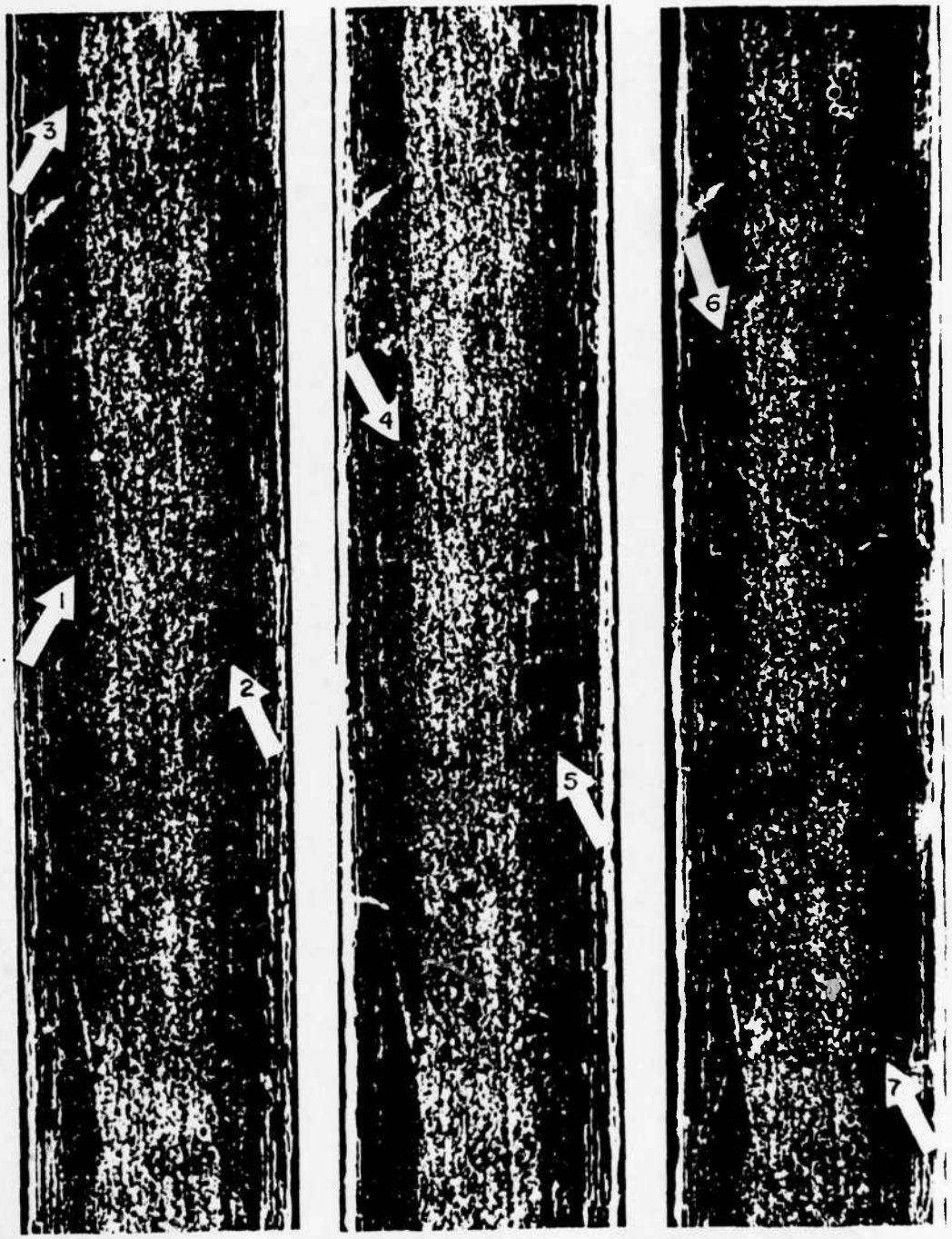

a) Static b) 50 Cycles c) 10 000 Cycles

Fig. 13 Replicas of 1600 lb, Type II Specimen

a) Static b) 50 Cycles c) 10 000 Cycles

Fig. 14 Replicas of 2000 lb, Type II Specimen

two of the transverse cracks present. The long black line is not a defect in the specimen, but is a deep scratch in the replica. After just 50 cycles (Fig. 14b), an extremely large number of cracks have formed. Many of these are spaced at a distance roughly equivalent to the thickness of one individual layer. A few of the cracks have even grown into the adjacent 45° layers (arrows 3 and 4). This characteristic was also observed in the Type I specimens. It appears that few, if any, additional transverse cracks had formed in the 90° layers by 10,000 cycles (Fig. 14c), even though this is difficult to determine precisely due to the poor quality of this photograph. Of great interest, however, are the small delaminations that have begun to grow along the +45°/-45° interfaces (arrows 5 and 6). At arrow 6 there is even a small transverse crack beginning to develop in the inner -45° layer. The branch delaminations in the Type I specimens grew along the same +45°/-45° interfaces.

Figure 15 is of two different areas on this same 2000 lb specimen after 10,000 cycles. The arrow on (a) indicates one of the three transverse cracks through the inner -45° layers. These cracks are connected to cracks through the outer +45° layers by the +45°/-45° interface delaminations. This combination of cracking involves six of the eight layers of the specimen. Figure 15b is of an area near the tabs. These are the only regions in which such extensive longitudinal cracking occurs. This may be caused by an unresolved moment created by shear stresses between the grip wedges and the tabs.

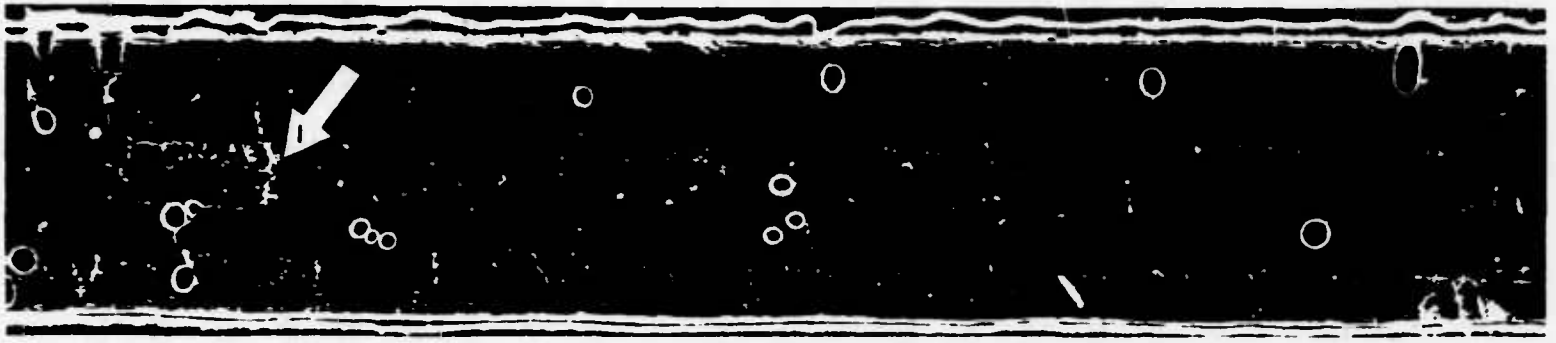

a) 10 000 Cycles

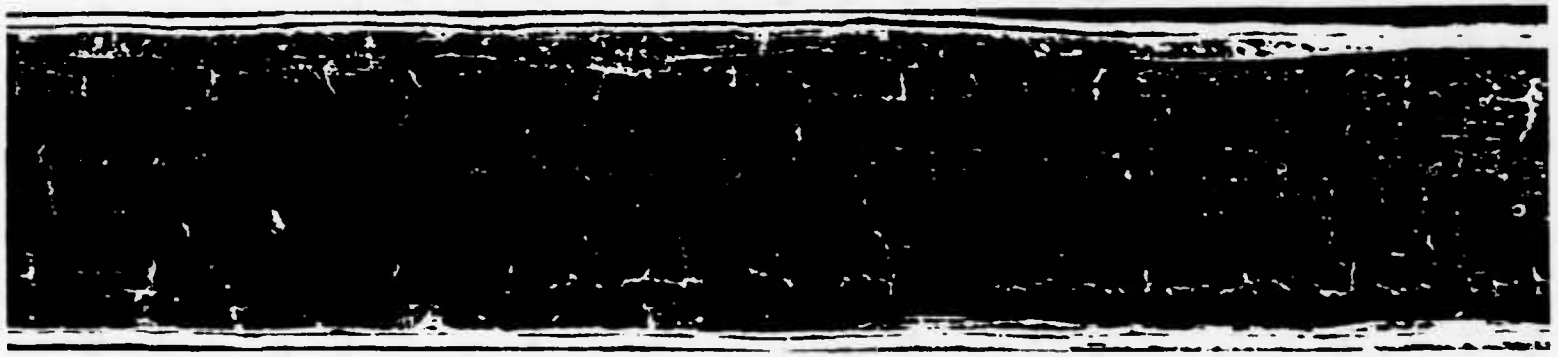

b) 10 000 Cycles

Fig. 15 Replicas of 2000 lb, Type II Specimen

After a static preload of 2700 lb, there is extensive cracking in the 90° layer (Fig. 16a). In addition, there are many cracks through the outer +45° layers and at least five cracks through the inner -45° layers, one of which is indicated by arrow 1. In Fig. 16b, after 50 cycles, it can be seen that the cracks in the 90° layers have opened up and have become more obvious, but there appear to be few, if any, additional cracks. The same holds true for the cracks in the outer +45° layers. Two new cracks have formed in the inner -45° layers. The spacing of these cracks is very similar to the spacing of the transverse cracks in the 90° layers for the Type I specimens. After 500 cycles, little change has taken place. The cracks seemed to have opened up slightly and some additional delamination has grown along the +45°/-45° interface (arrow 2).

As was the case for the Type I material, these replicas provided very consistent and detailed information concerning the types of edge damage, their interactions, and a chronological ordering of their development. This knowledge is essential to understanding the behavior of these materials.

5.2 Vibrothermography Results

The results of the vibrothermography technique were very conclusive in terms of locating delaminations in the x-y plane and making observations on their growth. Vibrothermography of Type II specimens indicated no unusual hot areas. This supports the observations made from the replicas that no delaminations occurred along the free edges.

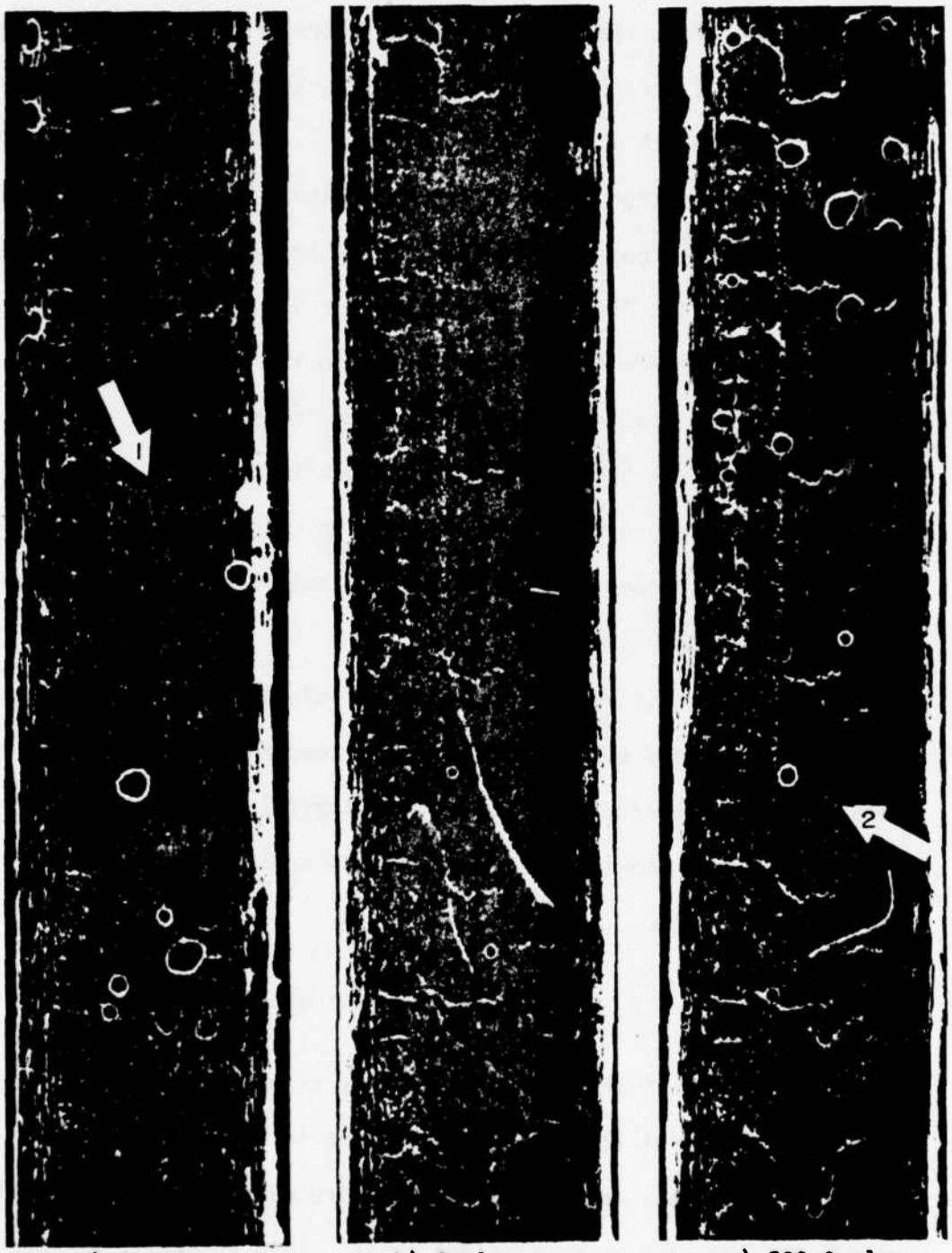

a) Static b) Cycles c) 500 Cycles

Fig. 16 Replicas of 2700 lb, Type II Specimen

However, vibrothermography of Type I specimens indicated numerous hot areas, all located along areas adjacent to the free edges (Fig. 17). These thermographs were made on a 2°C scale. A color band at the bottom of the figure indicates the color sequence in which each color represents a temperature of 0.2°C warmer than the color on its left. The large white areas or hot areas at the bottom of (a), (b), (c), and (f) represent heat from the gripping device of the ultrasonic transducer.

Figure 17a is of the 1600 lb specimen taken after 10,000 cyles. By comparing the hot areas between this and (c), the 2000 lb specimen after the same number of cycles, it can be seen that the higher load greatly increases the delaminated area. Thermograph (b) is of the 2000 lb specimen after the static preload but before fatigue. The absence of hot areas in this picture indicates that the fatigue cycling greatly increases the amount of delamination, (c). It was observed from the replicas that the edges contained extensive delaminations after the 2000 lb static preload; however, (b) does not indicate this. The reason for this may be that the delaminations were very shallow, confined very close to the edge, and therefore not detectable. After 10,000 cycles, the replicas indicated that there was a small increase in the total length of the delaminations but probably of more significance is their inward (through the width) growth. This would explain the reason for the discrepency between thermograph (b) and the replicas.

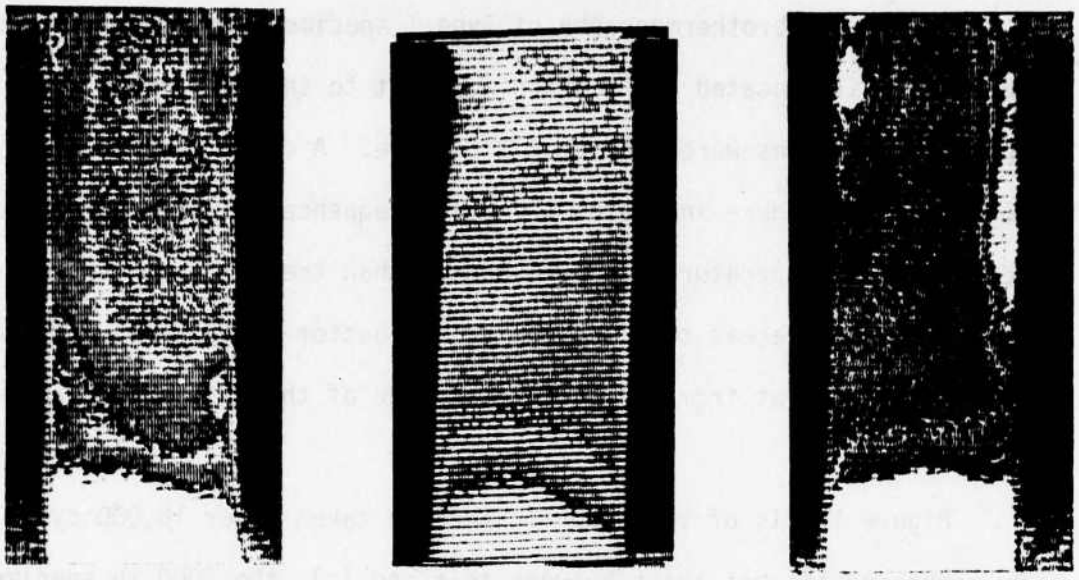

a) P=1600, n=10K b) P=2000, n=1 c) P=2000, n=10K

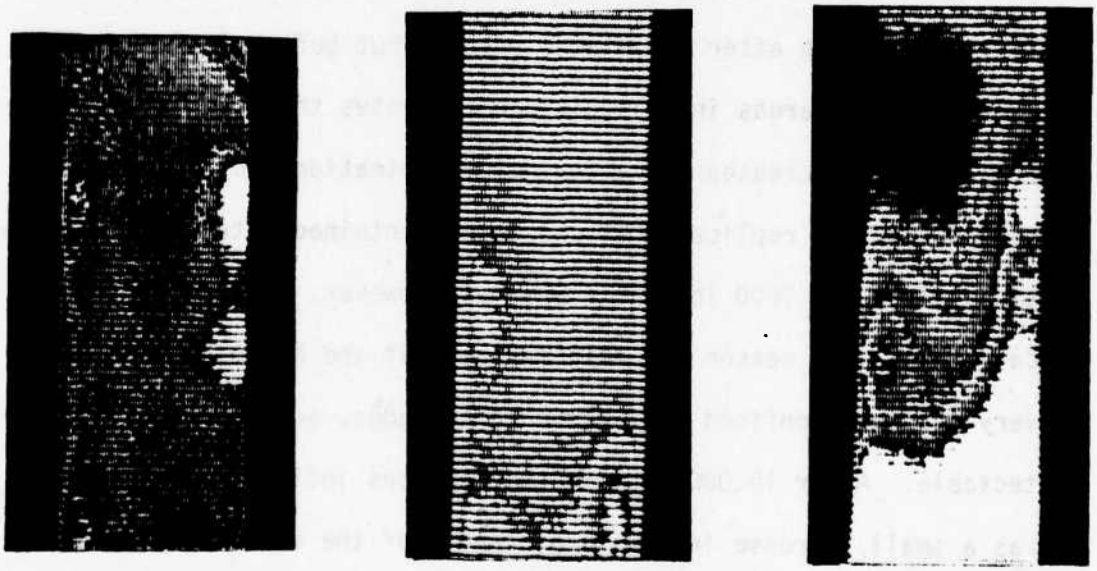

d) P=2700, n=1 e) P=2700, n=500 f) P=2700, n=500

Fig. 17 Thermographs of Type I Specimens

Thermograph (d) illustrates the degree of delamination due to a 2700 lb static preload. It shows considerable damage whereas the 2000 lb statically loaded specimen shows no significant damage. To add to the confusion of making comparisons, thermograph (d) has been taken of the opposite side of the specimen from (e) and (f). Therefore, its right side corresponds to the left side of (e) and (f). Thermographs (e) and (f) are both of the 2700 lb specimen after 500 cycles but they are taken at different frequencies. Comparisons between the before and after fatigue cases are not very apparent and it is therefore difficult to make any conclusions concerning the delamination growth from these last three prints.

In summary, this technique clearly distinguishes between Type I and Type II specimens. Also, it appears to be capable of indicating a relative degree of delamination damage with respect to growth in the x-y plane.

5.3 Characteristics of Specimen Failures

A portion of this research effort was to investigate the fracture area of each specimen, observe any characteristic behavior, and determine if fracture occurred along cracking that had been previously recorded. After the fatigue cycling was completed, each specimen was statically loaded to failure. The fractured edges were replicated and then used to determine the exact location of the fracture from the post-fatigue replicas.

It was observed that both Type I and Type II specimens fractured according to characteristic patterns. Figure 18 contains sketches of these patterns. For both types, the long delaminations occurred along the $+45^{\circ}/-45^{\circ}$ interfaces. The finite element analysis yielded high τ_{xz} stresses near the free edges along these interfaces. In addition, for all six specimens, the cracks between the long delaminations and the outside edges were approximately across from each other. The average length of the sections that pulled out or separated for the Type II specimens were considerably longer than those of Type I. Pulled out sections for the Type I materials varied from 0.132-0.224 in. in length and from 0.289-0.553 in. for Type II. Type II specimens contained a central delamination originating from the tip of the pulled out section. This was probably caused by shear stresses acting along the long delaminations as the sections were pulled apart. The same phenomena may have occurred in Type I specimens, however, it would not have been observed since the material contained extensive delaminations prior to failure.

Only one specimen, the 2000 lb Type I specimen, fractured along previously observed cracks. For this case, a transverse crack and its long branch delaminations (Fig. 10b) formed the top of the section that separated. The fracture lines ran along the two $+45^{\circ}/-45^{\circ}$ interfaces for 0.224 in. before breaking through the outer layers (arrows 5 and 6, Fig. 9c). It can be seen at arrow 5 that a crack already existed through the outer 45° layer prior to failure. This observation suggests that fracture may be edge dominated; however,

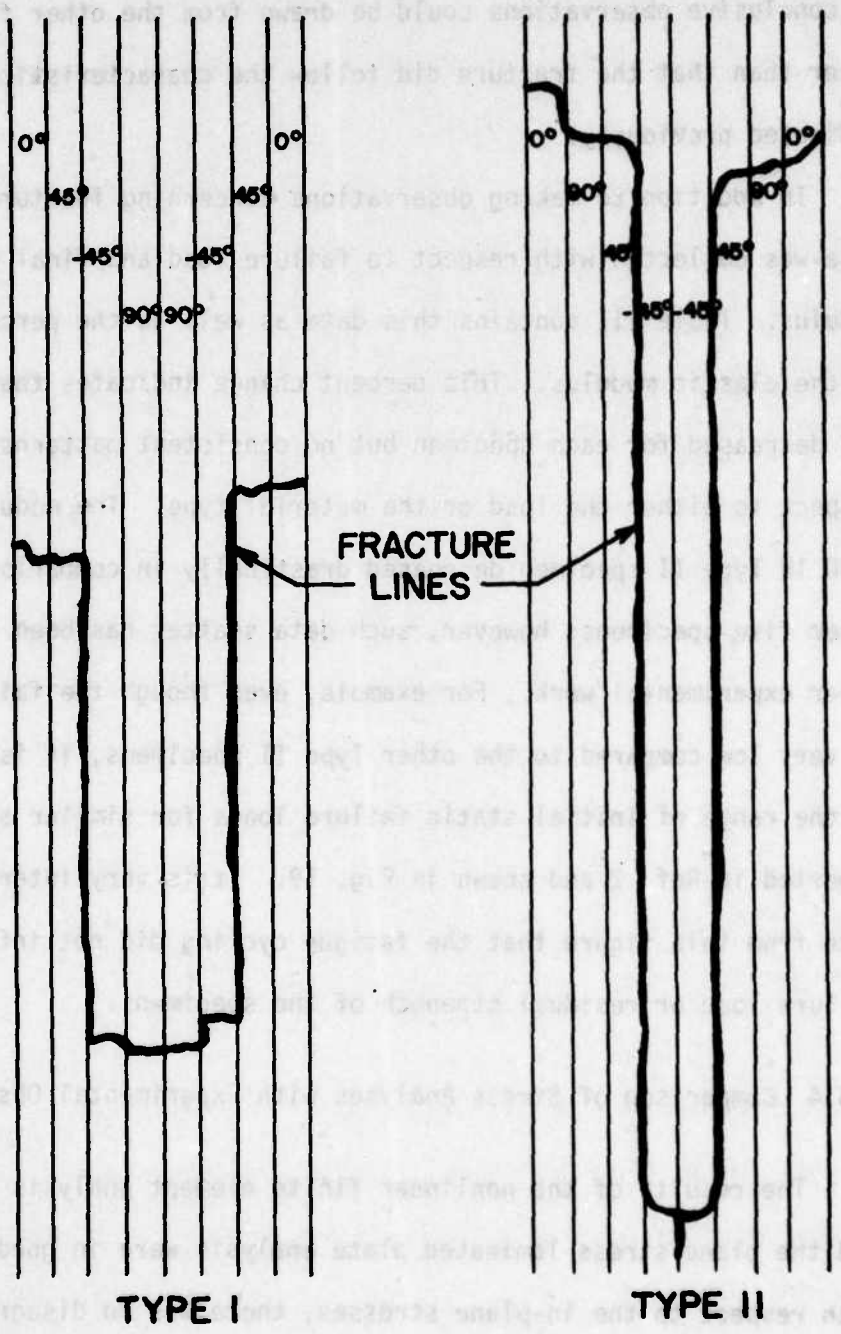

Fig. 18 Typical Edge View Fracture Patterns for Type I and Type II Specimens

no conclusive observations could be drawn from the other five specimens other than that the fracture did follow the characteristic patterns as indicated previously.

In addition to making observations concerning fracture patterns, data was collected with respect to failure load and final elastic modulus. Table III contains this data as well as the percent change in the elastic modulus. This percent change indicates that the modulus decreased for each specimen but no consistent patterns exist with respect to either the load or the material type. The modulus of the 2700 lb Type II specimen decreased drastically in comparison to the other five specimens; however, such data scatter has been observed in other experimental work. For example, even though the failure load is very low compared to the other Type II specimens, it is still within the range of initial static failure loads for similar specimens as reported in Ref. 2 and shown in Fig. 19. It is very interesting to note from this figure that the fatigue cycling did not influence the failure load or residual strength of the specimens.

5.4 Comparison of Stress Analyses with Experimental Observations

The results of the nonlinear finite element analysis (Ref. 12) and the plane stress laminated plate analysis were in good agreement. With respect to the in-plane stresses, there was no disagreement in stresses greater than 10.6 percent for Type I material and 7.1 percent for Type II material with an axial load of 2000 lb. Generally, the agreement was within three percent. Also, there was excellent

Table III. Initial and Final Properties

	Load Level	E_o	E_f	ΔE(3)	P_f	A	ϵ_f
Type	(lb)	(10^6 psi)	(10^6 psi)	(%)	(lb)	(in^2)	(%)
I	1600	6.197(1)	5.855	-5.52	2950	.0468	1.077(2)
I	2000	6.218	5.702	-8.30	3080	.0471	1.147(2)
I	2700(4)	6.160	5.718	-7.18	3260	.0478	1.193(2)
II	1600	6.508	6.053	-6.99	3650	.0461	1.308
II	2000	6.427	6.038	-6.05	3800	.0472	1.339
II	2700(4)	6.627(1)	5.728	-13.57	3270	.0467	1.222(2)

(1) Measured with extensometer, all other measurements were with strain gages.

(2) Determined from P_f and E_f, assuming linear to failure.

(3) $\% \Delta E = (E_f - E_o)/E_o \times 100$.

(4) Fatigued for 500 cycles, all others fatigued 10,000 cycles.

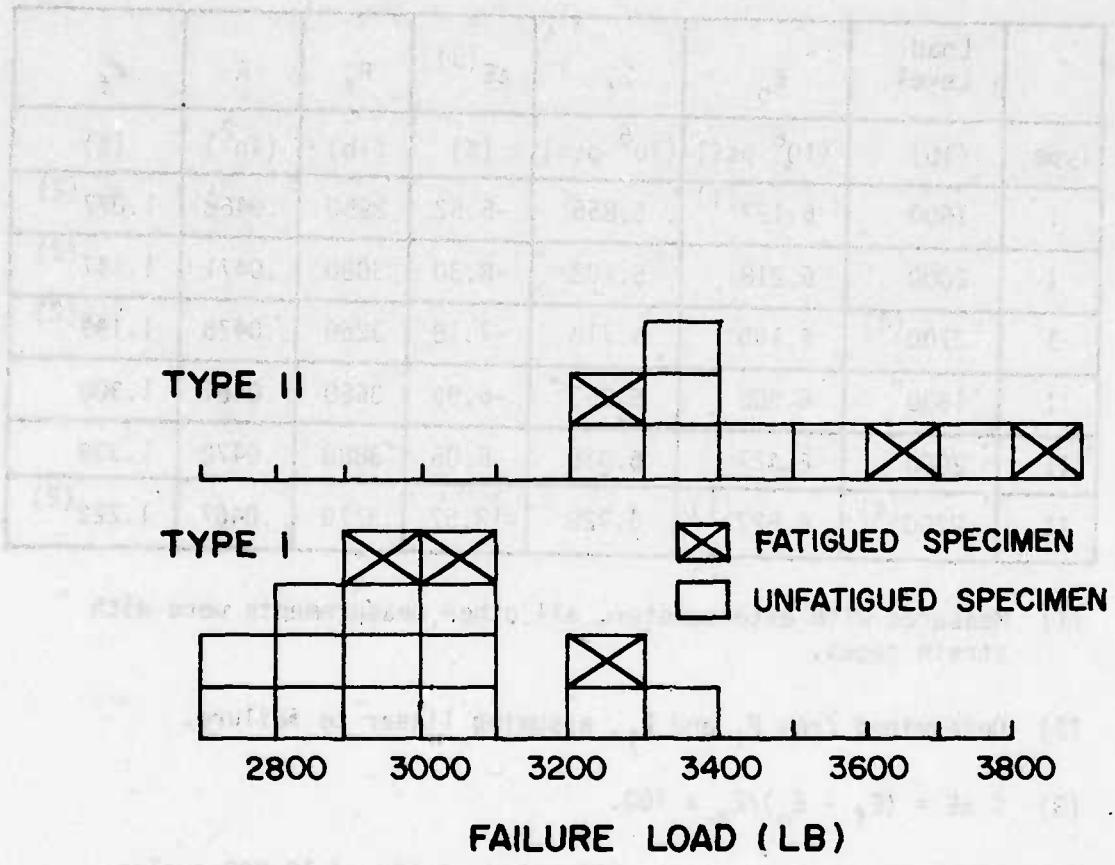

Fig. 19 Distribution of Failure Loads for Type I and Type II Specimens

agreement between the interlaminar normal stress, σ_z, as determined by the approximate method (Ref. 11) and by the finite element method (Fig. 20, 21, 23, and 24). For the purpose of this investigation, the main advantage of the finite element analysis was that it calculated interlaminar shear stresses. The advantage of the laminated plate analysis was that it required much less data and was not as expensive to run. It required less than one second of computer time as compared to four minutes for the finite element analysis.

5.4.1 Type I Specimens

The first damage observed in the Type I specimens was transverse cracking in the two middle 90° layers. After the static load, the 1600 lb specimen had about 8-10 cracks per inch. If the σ_x stresses in the 90° layers are primarily responsible for this damage, then at 1600 lb. the stresses must be relatively high in comparison to the strength of the 90° layers. This strength is about 7-8 ksi for unidirectional material. The analysis predicts a stress of 12.2 ksi at a 1600 lb axial load. Even with such non-rigorous reasoning, it is apparent that the 90° layers are heavily overloaded.

Delaminations begin almost as soon as the transverse cracking. The vibrothermography results agree with the observations of other researchers (Ref. 14), that delaminations initiate at the free edges. Three of the six stress components, σ_y, τ_{xy}, and τ_{yz}, must be zero at the free edge. Only two, σ_z and τ_{xz}, were shown by the analyses to be significantly higher at the edges than at interior regions.

Figure 20 is a graph of the through-the-thickness σ_z stress distribution near the free edge. The approximate method yields stresses at the edge, but the finite element solution gives the stress at a point which is .008 in. from the edge (or y/b = .983 where b is the half width). Note that due to the sharp gradient, the finite element values at this point are only 28.5 percent of the approximate values at the edge. These stresses are tensile along the entire laminate edge and will tend to cause delamination. The highest stresses occur in the regions near the midplane, which, as indicated by the replicas, are most susceptible to delamination. Figure 21 shows that the σ_z stresses are confined to a layer region adjacent to the edge. Some delamination was observed in the 1600 lb specimen after its static preload. In this case, σ_z stresses of 11.2 ksi were predicted along the midplane at the edge. This would indicate that, if σ_z is primarily responsible for delamination, the interlaminar normal stress must be kept well below 11 ksi to prevent delamination. Reference 2 is in close agreement with this statement in its prediction of 10 ksi as being sufficient to initiate delamination.

Figure 22 shows the through-the-thickness τ_{xz} stress distribution at 0.008 in. from the edge. For the Type I material, these shear stresses peak at the $+45^{\circ}/-45^{\circ}$ interface. This is the same interface along which the branch delaminations were observed. They were first noticed after the 1600 lb static load; however, it required either higher static loads or cyclic loads to cause them to grow to any significant length. At 1600 lb, the σ_z stress at this

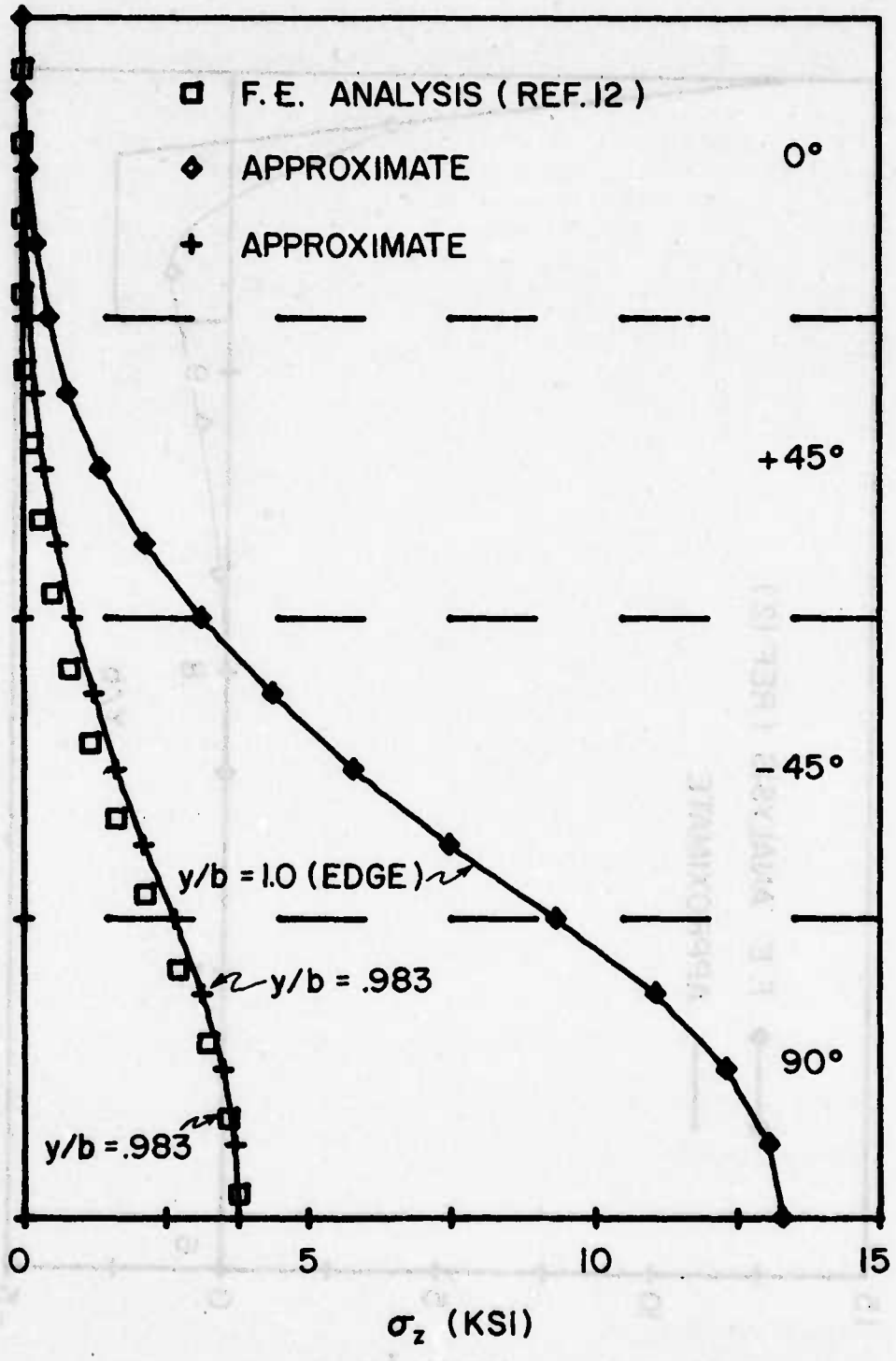

Fig. 20 Interlaminar Normal Stress, σ_z, Through-the-Thickness Distribution for a Type I Specimen with 2000 lb Axial Load

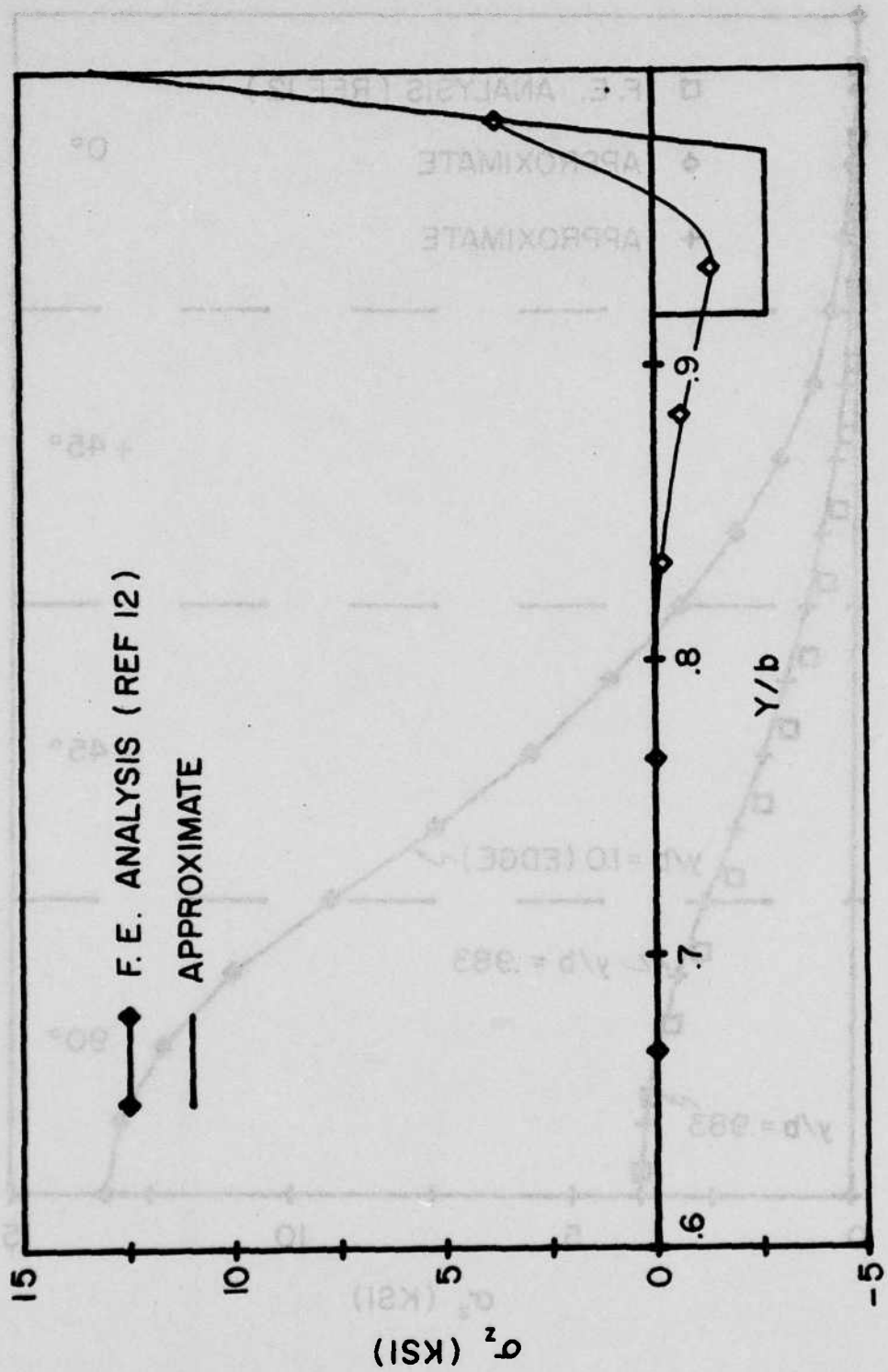

Fig. 21 Interlaminar Normal Stress, σ_z, Through-the-Width Distribution for a Type I Specimen with 2000 lb Axial Load

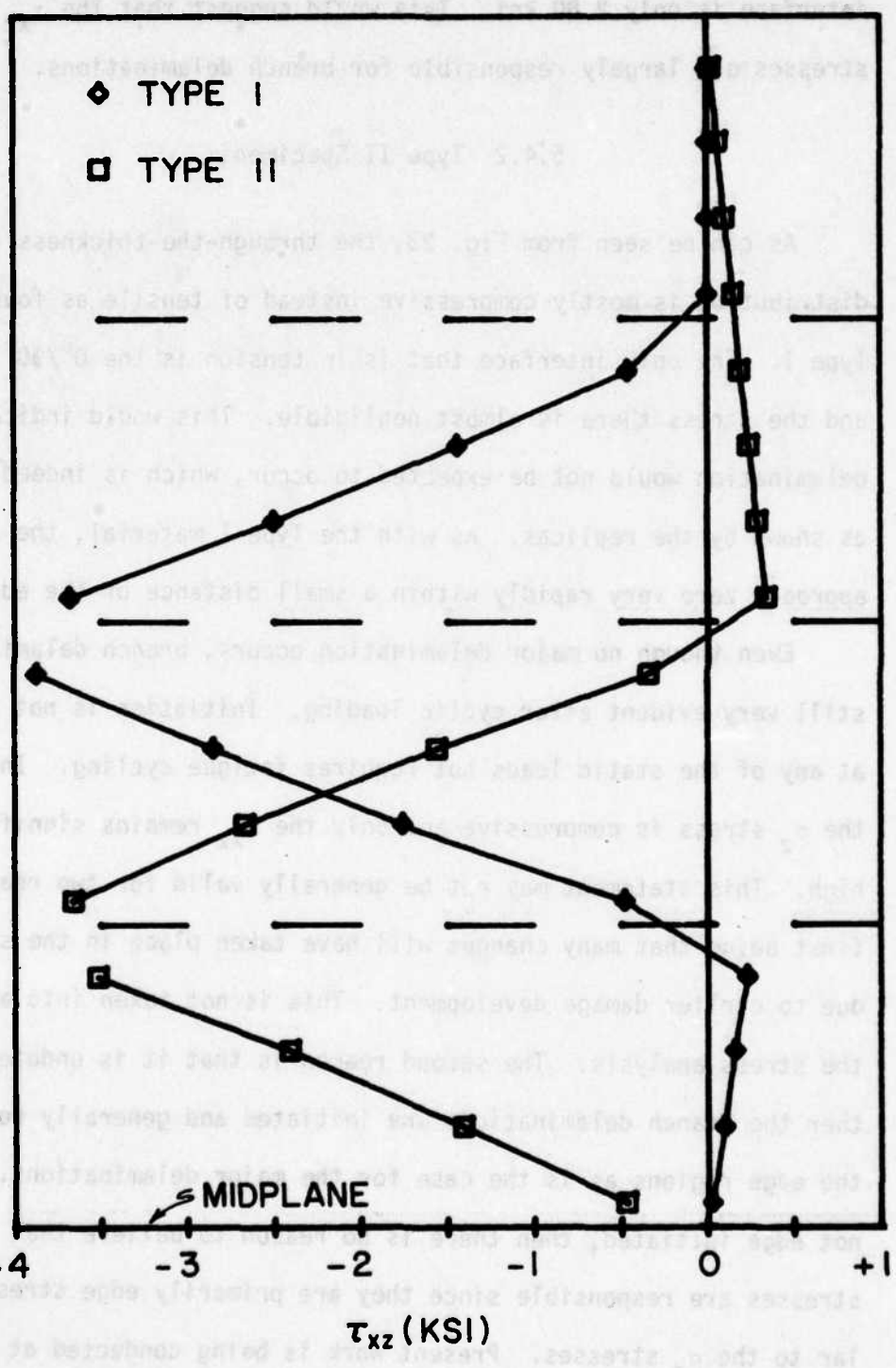

Fig. 22 Interlaminar Shear Stress, τ_{xz}, Through-the-Thickness Distribution at y/b = .983 with 2000 lb Axial Load

interface is only 2.80 ksi. This would suggest that the τ_{xz} shear stresses are largely responsible for branch delaminations.

5.4.2 Type II Specimens

As can be seen from Fig. 23, the through-the-thickness σ_z stress distribution is mostly compressive instead of tensile as found with Type I. The only interface that is in tension is the $0^\circ/90^\circ$ interface, and the stress there is almost negligible. This would indicate that delamination would not be expected to occur, which is indeed the case, as shown by the replicas. As with the Type I material, the σ_z stresses approach zero very rapidly within a small distance of the edge (Fig. 24).

Even though no major delamination occurs, branch delamination is still very evident after cyclic loading. Initiation is not accomplished at any of the static loads but requires fatigue cycling. In any case, the σ_z stress is compressive and only the τ_{xz} remains significantly high. This statement may not be generally valid for two reasons. The first being that many changes will have taken place in the stresses due to earlier damage development. This is not taken into account by the stress analysis. The second reason is that it is undetermined whether the branch delaminations are initiated and generally confined to the edge regions as is the case for the major delaminations. If it is not edge initiated, then there is no reason to believe that τ_{xz} stresses are responsible since they are primarily edge stresses similar to the σ_z stresses. Present work is being conducted at VPI&SU that should answer many questions concerning damage development at

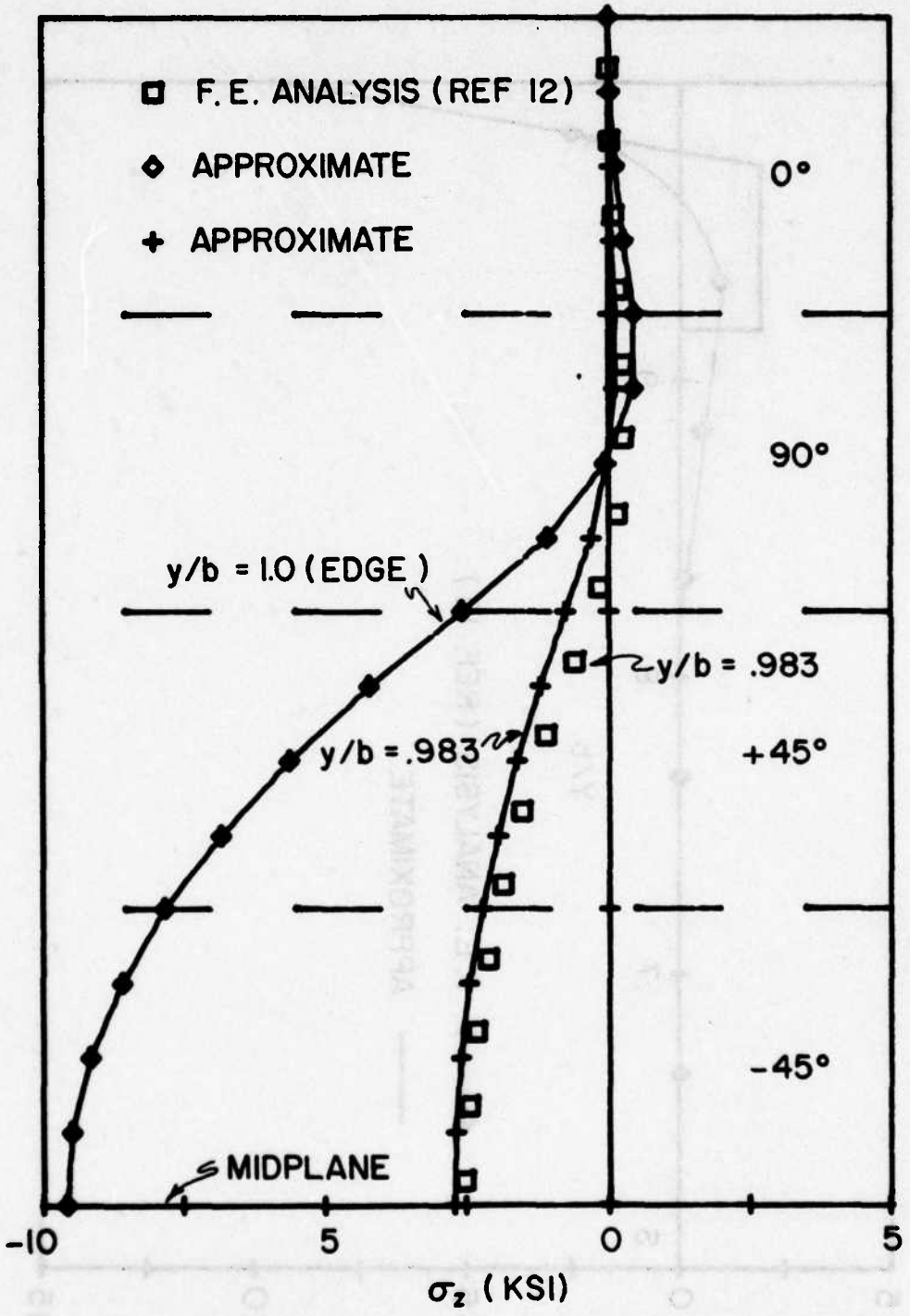

Fig. 23 Interlaminar Normal Stress, σ_z, Through-the-Thickness Distribution for a Type II Specimen with 2000 lb Axial Load

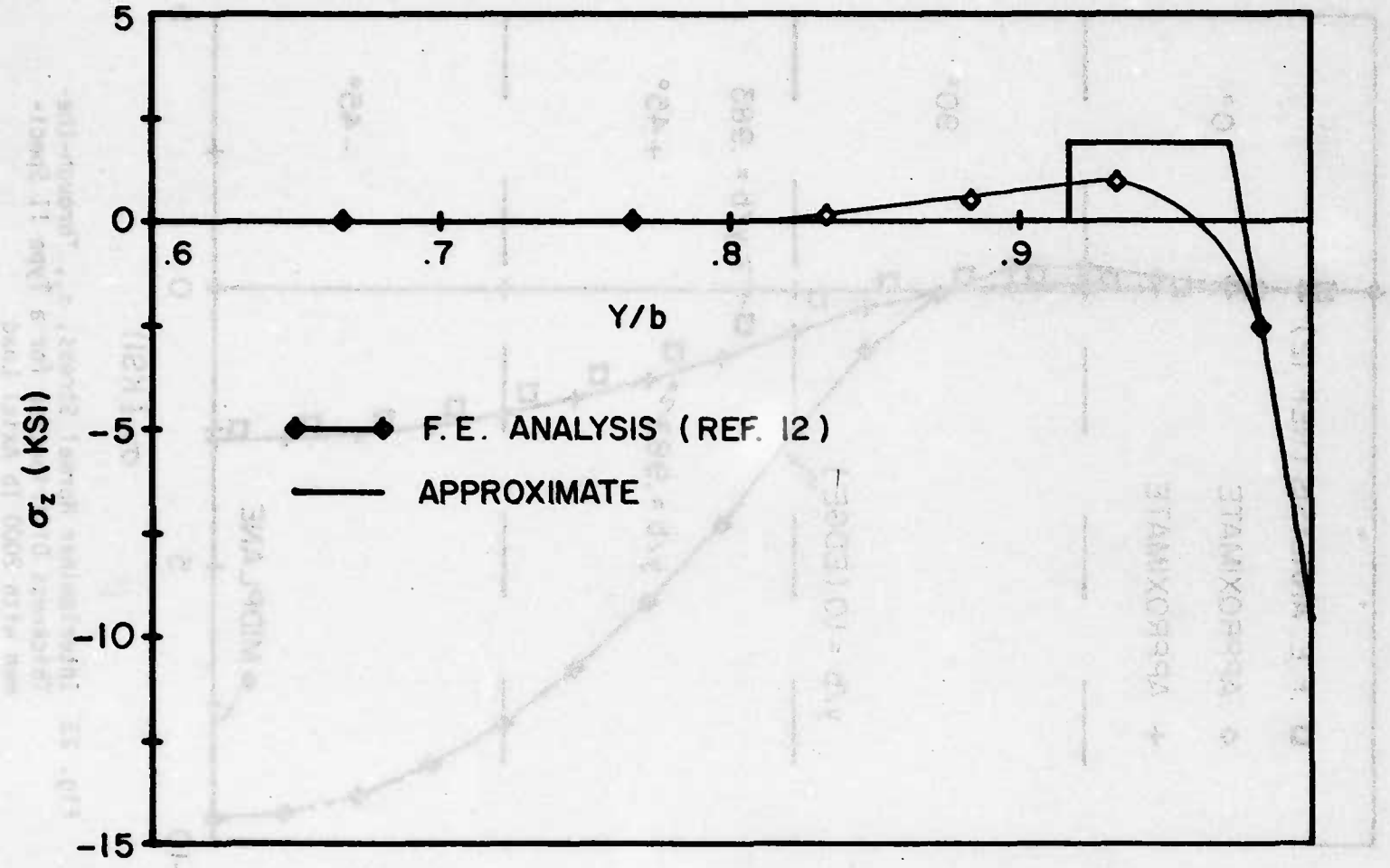

Fig. 24 Interlaminar Normal Stress, σ_z, Through-the-Width Distribution for a Type II Specimen for a Type II Specimen with 2000 lb Axial Load

interior regions. In conclusion, this investigation tends to indicate that the τ_{xz} shear stresses are primarily responsible for branch delaminations.

Many of these comparisons between the predicted stresses and the observed damage have been non-rigorous. These analyses were performed to help get a "handle" on the causes of the different types of damage. This information is essential to the improvement of the design capabilities for these types of materials.

6. Summary

The purpose of this investigation was to develop a method of accurately documenting the effect of load history on damage development in two types of graphite/epoxy composites and to provide a detailed description of damage initiation, growth, and interaction. Characterizations of fracture due to static load were observed and compared to pre-existing damage. Comparisons were made between the states of damage caused by static loads below, approximately equal to, and above the load which corresponded to the axial stress-strain knee.

Many interesting characteristics of edge damage in quasi-isotropic G/Ep laminates have been observed through the use of the replication technique that have not been reported previously. Transverse cracking in the 90° layers, hooked cracks in the adjacent 45° layers, and branch delaminations along the $+45^{\circ}/-45^{\circ}$ interfaces are types of damage that were found to be common in both Type I and Type II materials. Transverse cracking through the middle -45° layers was found only in Type II materials and major delaminations were found only in Type I materials.

The density of transverse cracks in the 90° layers of Type I specimens appeared to stabilize by at least, if not before, 10,000 cycles at 1600 lb, 500 cycles at 2000 lb, and the static preload at 2700 lb. These cracks demonstrated a relatively stabile spacing; varying from the laminate thickness to a third of the thickness. Hooked cracks, in the adjacent 45° layers, were initiated by the initial 1600 lb preload. A large majority of these branched from

the 90° transverse cracks. Central delaminations also began at or before the initial 1600 lb static load. These appeared to initiate due to longitudinal cracking, most of which was associated with transverse cracking. The delaminations were confined to the region of the inner 90° layers. If a delamination along the middle interface grew into a transverse crack it either: 1) was temporily stopped by the crack, in which case it accelerated the growth of the branch delaminations associated with that crack, or 2) continued straight through the crack. If a delamination along either of the 90°/-45° interfaces grew into a transverse crack it generally jumped to the opposite 90°/-45° interface before continuing its growth. In all three specimens it was noted that no new transverse cracks formed along any area of the edge that had previously delaminated. For all three load levels, delaminations were present at the static preloads. After 10,000 cycles at 1600 lb the edge was approximately 92 percent delaminated as compared with 97 percent for the same number of cycles at 2000 lb and 100 percent for 500 cycles at 2700 lb. After the edge completely delaminated, the delamination crack opening or width began increasing rapidly.

In Type II materials the first damage that occurred was also transverse cracking in the 90° layers. These cracks were only one half of the length of those in Type I and the crack opening was much smaller. The crack density stabilized by at least, if not before, 50 cycles at 2000 lb and the static preload at 2700 lb. No stabile density was observed for the 1600 lb specimen. After obtaining a stabile crack density, a spacing of about the thickness of one layer

was observed between the cracks. Hooked cracks through the adjacent 45° layers were initiated by the 1600 lb static load and their crack density appeared to stabilize along with the 90° cracks. The growth of branch delaminations in the $+45^{\circ}/-45^{\circ}$ interfaces was observed after the 90° and 45° layer cracking had reached a stabile density. No major delaminations, which were so evident in Type I material, were observed. Transverse cracking in the inner -45° layers was the last damage mode to be initiated. It was first observed after 10,000 cycles at 2000 lb or after the static preload at 2700 lb and its growth became stabile after 50 cycles at 2700 lb.

The knee in the axial stress-strain curve occurs in the neighborhood of 2000 lb. Micromechanical damage in the form of transverse cracks begins well before this load as demonstrated by the replicas of the 1600 lb specimens. The only significant edge damage development that might be associated with the knee is the obtaining of a stabile density of the 90° layer transverse cracks. In both Type I and the Type II 2000 lb specimens, the crack density did not actually stabilize after the static preload; however, it quickly became stabile after a small number of cycles. Therefore, if reaching the stabile crack density is responsible for the knee, then the knee would have occurred at a slightly higher load than 2000 lb.

Characteristic edge patterns were determined for the fracture of both types of materials. The large central delaminations that occurred in Type I material had no affect on the fracture pattern. For both materials the fracture lines ran along the $+45^{\circ}/-45^{\circ}$

interfaces. These were the same interfaces in which branch delaminations were observed. In Type I material, the long fracture lines joined a 90° layer transverse crack, with its two associated hooked cracks, to other cracks in the outer 45° layers. In the Type II materials, these long fracture lines joined an inner -45° layer transverse crack to other hooked cracks in the outer 45° layers and their parent 90° layer transverse cracks. The fracture locations could be related to pre-existing damage in only one of the six specimens. The 0° layers did not appear to crack until all other layers were fractured. Residual strengths of the specimens did not seem to be affected by cyclic loading even though there was considerable scatter in this data as well as the unfatigued specimen data. However, the elastic modulus was greatly influenced by fatigue. It decreased in all six cases by amounts varying from 5.5 to 13.6 percent.

Two different stress analyses were used to determine the stress fields in each of the two types of materials. The first analysis was based on plane-stress laminated plate theory with compensation for curing stresses and an approximate technique for determining interlaminar normal stresses. The second analysis was a finite element analysis which used non-linear stress-strain properties and compensated for the change in properties with respect to temperature in the calculation of curing stresses. All six components of stress were determined. The in-plane stresses from the two analyses were very close; in no case differing by more than ten percent. Interlaminar normal stresses were almost identical. If interlaminar shear stresses

are not needed, the approximate analysis serves as a very inexpensive and quick method of obtaining a good first approximation of the stresses.

The results of the stress analysis can serve to predict some of the observed damage. Tensile interlaminar normal stresses, σ_z, at the edges are primarily responsible for the delamination of a laminate. High τ_{xz} shearing stresses (3-4 ksi) along the $+45^\circ/-45^\circ$ interfaces (0.008 in. from the free edge) appear to be responsible for branch delaminations even in the presence of compressive σ_z stresses.

Some basic information concerning the growth of delamination in Type I specimens was obtained from the vibrothermography technique. It indicated that delamination was initiated at the free edges and became more extensive with the increase of either the stress level or the number of cycles of fatigue. The delaminations appeared to grow inward as well as along the edges. No delamination could be detected in Type II specimens.

7. Conclusions

The observations that were made and the information that was learned through this research effort suggest the following conclusions:

1) The replication technique developed for this investigation is a quick, reliable method of permanently documenting edge damage. It provides detail and an overall field of vision that has not been obtained in previous studies.

2) Vibrothermography is an effective method of detecting delaminations and following their growth in the plane of the specimen.

3) The ultrasonic pulse-echo method needs to be studied in closer conjunction with the replication technique. It must be determined what effects the transverse cracks under the transducer have on the measured attenuation.

4) The "at load" damage investigation reveals considerable amounts of micromechanical damage at stress levels below the proportional limit.

5) A chronological order of damage occurrences was established for each laminate. Damage initiation, growth, and interaction is strongly dependent on the order of the stacking sequence.

6) Some types of damage, such as transverse cracking of the 90° layers, eventually reach a stabilized state. Other types, such as branch and major delaminations, were not observed to stabilize within the limits of this investigation.

7) Distinct but different characteristics or patterns of fracture were observed for the two laminates.

8) The ultimate strength of the specimens did not appear to be influenced by the cyclic loading. However, the elastic modulus decreased.

9) The approximate stress analysis gave a very good estimate of the stress distribution when compared to the finite element method. In particular, the σ_z stresses were very close.

10) Major delaminations were primarily caused by tensile σ_z stresses along the edge. Branch delaminations are suspected of being caused by high τ_{xz} shearing stresses along the $+45^{\circ}/-45^{\circ}$ inferfaces near the free edges.

Many of these conclusions could be further verified by the investigation of a third stacking sequence; for example, $[0, +45, 90, -45]_s$. The stress analyses would be used to predict the types of damage and their locations, then the accuracy of the predictions checked through the use of the replication technique. More work needs to be done to refine this technique. Better solvents need to be found, photographic reproduction methods improved, and specimen surfaces polished. With more study concerning the development of damage at interior regions of the specimens it may be possible to relate edge damage to interior damage. This would be ideal in that the state of damage of the entire specimen could be determined by simply observing the damage present along the free edges. Finally, the time-dependent behavior of edge damage should be studied by conducting this investigation at a different frequency.

This investigation has been relatively specific in that only two laminates were studied and only six specimens used. However, much of the information that has been gained may apply for composites in general. Hopefully, future investigations will be assisted through these conclusions. Certainly the replication technique is one that can have a wide variety of applications in the damage study of composites. A knowledge of the microscopic damage development of a composite is essential to the understanding of its macroscopic behavior.

References

1. Grimes, Glenn C., "Structural Design Significance of Tension-Tension Fatigue Data on Composites," Composite Materials: Testing and Design (Fourth Conference), ASTM STP617, American Society for Testing and Materials, 1977.

2. Reifsnider, K. L., Henneke, E. G., Stinchcomb, W. W., "Defect-Property Relationships in Composite Materials," Technical Report AFML-TR-76-81, Air Force Materials Laboratory, Dayton, Ohio, 1976.

3. "Hercules Product Data," Sheet #832, Hercules Incorporated, Wilmington, Delaware.

4. Composites Design Guide, 3rd ed., Advanced Development Division, Air Force Materials Laboratory, Dayton, Ohio, Vol. 14, Section 4.1.1-3.11.A, September 1976, pp. 14-16.

5. Whiteside, J. B., private communication.

6. Jones, T. S., "Thermographic Detection of Damaged Regions in Fiber-Reinforced Composite Materials," M. S. Thesis, Virginia Polytechnic Institute and State University, Blacksburg, Virginia, 1977.

7. Jones, Robert M., Mechanics of Composite Materials, McGraw-Hill, New York, 1975, pp. 31-55, 147-165, 193-198.

8. Hahn, H. T. and Pagano, N. J., "Curing Stresses in Composite Laminates," Journal of Composite Materials, Vol. 9, January 1975, p. 91.

9. Pagano, N. J. and Pipes, R. B., "The Influence of Stacking Sequence on Laminate Strength," Journal of Composite Materials, Vol. 5, January 1971, p. 50.

10. Pipes, R. B., Ph.D. dissertation, University of Texas, Arlington, March 1972.

11. Pagano, N. J. and Pipes, R. B., "Some Observations on the Interlaminar Strength of Composite Materials," International Journal of Mechanical Science, Vol. 15, 1973, pp. 679-688.

12. Renieri, G. D. and Herakovich, C. T., "Nonlinear Analysis of Laminated Fibrous Composites," Technical Report VPI-E-76-10, Virginia Polytechinc Institute and State University, Blacksburg, Virginia, June 1976.

13. Humphreys, E. H., "Nonlinear Analysis of Bonded Joints with Thermal Effects," M. S. Thesis, Virginia Polytechnic Institute and State University, Blacksburg, Virginia, 1977.

14. Sendeckyj, G. P., "Fatigue Damage Accumulation in Graphite-Epoxy Laminates," Failure Modes in Composites-III, (ed. Chiao, T. T. and Shuster, D. M.), AIME, 1976, pp. 100-114.

Appendix A - Development of Curing Stress Equations

Section 4.1 presented in Eq. 6 and 7

$$[\sigma]^k = \Delta T\,[\bar{Q}]^T\,\{[\bar{\alpha}]-[\alpha]^k\} \tag{6}$$

where

$$[\bar{\alpha}] = h[A]^{-1}\sum_{k=1}^{n}[\bar{Q}]^k\,[\alpha]^k \tag{7}$$

as an approximate method to be used in combination with plane stress lamination theory to account for curing stresses. The formulation of these two equations begins by defining the strains as a function of ΔT for a unidirectional laminate as

$$\varepsilon_1^T = \alpha_1\,\Delta T, \tag{A1}$$

$$\varepsilon_2^T = \alpha_2\,\Delta T, \tag{A2}$$

and

$$\gamma_{12}^T = 0 \tag{A3}$$

where ΔT is the difference between the operating and stress-free temperature, α_1 and α_2 are the longitudinal and transverse thermal coefficients, respectively, and the "T" superscript denotes "thermal." This yields a combined thermal and mechanical strain for the unidirectional material of

$$[\varepsilon] = [\varepsilon^T] + [\varepsilon^M] \tag{A4}$$

where the "M" superscript denotes "mechanical." Combining Eq. 2 and A4 yields

$$\begin{Bmatrix}\sigma_1\\ \sigma_2\\ \tau_{12}\end{Bmatrix} = \begin{bmatrix}Q_{11} & Q_{12} & 0\\ Q_{12} & Q_{22} & 0\\ 0 & 0 & Q_{66}\end{bmatrix}\begin{Bmatrix}\varepsilon_1 - \alpha_1\Delta T\\ \varepsilon_2 - \alpha_2\Delta T\\ \gamma_{12}\end{Bmatrix} \tag{A5}$$

Transforming this to represent the stresses in the k^{th} layer of a laminate in a x-y coordinate system yields

$$\begin{Bmatrix} \sigma_x \\ \sigma_y \\ \tau_{xy} \end{Bmatrix}^k = [\bar{Q}]^k \begin{Bmatrix} \varepsilon_x - \alpha_x \Delta T \\ \varepsilon_y - \alpha_y \Delta T \\ \gamma_{12} - \alpha_{xy} \Delta T \end{Bmatrix}^k \tag{A6}$$

where $(\alpha_x, \alpha_y, \alpha_{xy})$ are the transformed thermal coefficients. The total strain components for a symmetric laminate are

$$[\varepsilon]^k = [\varepsilon^o], \tag{A7}$$

where $[\varepsilon^o]$ are the midplane strains. The midplane curvatures, $[\kappa]$, are zero since only symmetric laminates are being considered. Combining Eq. A6 and A7 and using and abbreviated form yields

$$[\sigma]^k = [\bar{Q}]^k \{[\varepsilon_o] - [\alpha]^k \Delta T\}. \tag{A8}$$

Recalling the definition of the laminate stress resultant from Eq. 5 and substituting Eq. A8 yields

$$[N] = \sum_{k=1}^{n} [\bar{Q}]^k \{[\varepsilon_o] - [\alpha]^k \Delta T\} h, \tag{A9}$$

where all layers are considered to be of an equal thickness, h, and n is the total number of layers. By defining the extensional stiffness matrix as

$$[A] = h \sum_{k=1}^{n} [\bar{Q}]^k, \tag{A10}$$

the stress resultant can be written as,

$$[N] = [A]\,[\varepsilon_o] - h\Delta T \sum_{k=1}^{n} [\bar{Q}]^k\,[\alpha]^k. \tag{A11}$$

As presented in Ref. 7, [N] can be written as

$$[N] = [\bar{N}] - [N^T], \tag{A12}$$

where

$$[\bar{N}] = [A]\,[\varepsilon_o] \tag{A13}$$

and

$$[N^T] = h\Delta T \sum_{k=1}^{n} [\bar{Q}]^k\,[\alpha]^k. \tag{A14}$$

$[N^T]$ represents the true thermal forces only if the laminate is perfectly constrained. However, if the laminate is unrestrained and subjected to thermal loading only, then

$$[N] = 0 \tag{A15}$$

and from Eq. A11

$$[\varepsilon_o] = h\Delta T\,[A]^{-1} \sum_{k=1}^{n} [\bar{Q}]^k\,[\alpha]^k. \tag{A16}$$

However, since the laminates considered are symmetric,

$$[\varepsilon_o] = [\bar{\alpha}]\,\Delta T, \tag{A17}$$

where $[\bar{\alpha}]$ are the laminate thermal coefficients. Eq. 7 can now be obtained from Eq. A16 and A17, and Eq. 6 from combining Eq. A17 and A8.

SECURITY CLASSIFICATION OF THIS PAGE (When Data Entered)

REPORT DOCUMENTATION PAGE		READ INSTRUCTIONS BEFORE COMPLETING FORM
1. REPORT NUMBER VPI-E-77-24	2. GOVT ACCESSION NO.	3. RECIPIENT'S CATALOG NUMBER
4. TITLE (and Subtitle) AN INVESTIGATION OF EDGE DAMAGE DEVELOPMENT IN QUASI-ISOTROPIC GRAPHITE EPOXY LAMINATES		5. TYPE OF REPORT & PERIOD COVERED 6. PERFORMING ORG. REPORT NUMBER VPI-E-77-24
7. AUTHOR(s) DAVID O. STALNAKER AND WAYNE W. STINCHCOMB		8. CONTRACT OR GRANT NUMBER(s) AFML F33615-75-C-5119
9. PERFORMING ORGANIZATION NAME AND ADDRESS Virginia Polytechnic Institute & State Univ. Department of Engineering Science & Mechanics Blacksburg, Virginia 24061		10. PROGRAM ELEMENT, PROJECT, TASK AREA & WORK UNIT NUMBERS
11. CONTROLLING OFFICE NAME AND ADDRESS Air Force Materials Laboratory Wright Patterson Air Force Base Ohio 45433		12. REPORT DATE September, 1977 13. NUMBER OF PAGES 89
14. MONITORING AGENCY NAME & ADDRESS(if different from Controlling Office) Virginia Polytechnic Institute & State Univ. Department of Engineering Science & Mechanics Blacksburg, Virginia 24061		15. SECURITY CLASS. (of this report) UNCLASSIFIED 15a. DECLASSIFICATION/DOWNGRADING SCHEDULE

16. DISTRIBUTION STATEMENT (of this Report)

Approved for public release, distribution unlimited.

17. DISTRIBUTION STATEMENT (of the abstract entered in Block 20, if different from Report)

18. SUPPLEMENTARY NOTES

19. KEY WORDS (Continue on reverse side if necessary and identify by block number)

Composite materials, fatigue, damage, delamination, quasi-isotropic, laminate, graphite epoxy, load-history effects.

20. ABSTRACT (Continue on reverse side if necessary and identify by block number)

See page ii

DD FORM 1 JAN 73 1473 EDITION OF 1 NOV 65 IS OBSOLETE

SECURITY CLASSIFICATION OF THIS PAGE (When Data Entered)


ATE
LMED